JOURNAL OF GEOPHYSICAL RESEARCH, VOL. 106, NO. C12, PAGES 31,263–31,282, DECEMBER 2001

On the mass and salt budgets for a region of the continental shelf in the southern Mid-Atlantic Bight

This paper was written with support of the U.S. Department of Energy under Contract No. DE-FG02-92ER61416. The Government reserves for itself and others acting on its behalf a royalty-free, nonexclusive, irrevocable, worldwide license for Governmental purposes to publish, distribute, translate, duplicate, exhibit and perform this copyrighted paper.

Yoo Yin Kim
Department of Meteorology, Florida State University, Tallahassee, Florida, USA

Georges L. Weatherly
Department of Oceanography, Florida State University, Tallahassee, Florida, USA

Leonard J. Pietrafesa
Department of Marine, Earth and Atmospheric Sciences, North Carolina State University, Raleigh North Carolina, USA

Abstract. Two field studies were conducted across and along the continental shelf, one from February to May 1996 (deployment 1) and the other from July to October 1996 (deployment 2) in part to determine the mass and salt budgets of shelf water from south of Cape Henry to north of Cape Hatteras, the southernmost portion of the Mid-Atlantic Bight. The temporal means of current meter records indicated that most of the water enters the region across its northern boundary near the shelf break as part of a southward, alongshore current and exits the southeast corner as a southeastward flowing current. Estimates of the volume transports indicated that not all the transport across the northern boundary was accounted for by transport across the southern boundary and that the remainder occurred as a broad, diffusive flow across the eastern boundary at the shelf break. Time series of volume transport across northern and southern boundaries were very similar and associated with variations in the alongshore wind stress and sea level, indicative of a geostrophic balance. Examination of the individual current meter records indicated these fluctuations were very barotropic even during deployment 2, which included the stratified summer season. Time series of the volume transport across the eastern boundary at the shelf break strongly mirrored the volume transport across the northern boundary minus that across the southern boundary, suggesting that the inferred eastern boundary transport was real and accommodated whatever the southern boundary could not. The turbulent salt flux across each boundary contributes very little to the net salt flux. The mean and time-dependent salt fluxes show nearly identical patterns as the respective mass fluxes because the salt fluxes are almost governed by current velocity fields. The instantaneous and mean salt fluxes across each boundary were very well approximated by the instantaneous and mean volume transports across the boundary times the deployment average salinity across that boundary, respectively. The Ocean Margins Program (OMP) moored current and salinity observations appear sufficient to make estimates of the mean and time-dependent mass and salt balance.

1. Introduction

We present some results about the time-averaged and daily time series of mass and salt fluxes, their balance, and the variability of mass and salt fluxes in a region on the continental shelf. The moored current and salinity data examined here were obtained from the Ocean Margins Program (OMP), a U.S. Department of Energy study conducted on the southernmost shelf of the Mid-Atlantic Bight (MAB).

An array of heavily instrumented and closely spaced moorings was set in the OMP region, which is north of Cape Hatteras and south of Cape Henry. For this study, data from moorings on the northern, eastern, and southern sides of the OMP region (Figure 1) were considered. The OMP experiments were conducted across and along the continental shelf from February to May 1996 and again from July to October 1996 (Figure 1). A primary aim was to quantify mass and salt fluxes in the OMP region (with the ultimate intent of quantifying the fluxes of organic carbons). The continental shelf water of the MAB has its widest range of temperature and salinity in its southern portion near Cape Hatteras [*Boicourt*, 1973; *Wright and Parker*, 1976; *Pietrafesa et al.*, 1994; *Churchill and Berger*, 1998]. There the shelf water is composed of coastal water from Chesapeake and Delaware Bays, water from the northern MAB shelf, and saline slope water from the offshore region owing to the proximity of the Gulf Stream.

In past years, considerable progress has been made in the study of mean circulation and its variability on the Mid-Atlantic Bight (Cape Hatteras to Cape Sable) through direct current meter measurements. Experiments were carried out in different regions: between Cape May and Cape Hatteras [*Boicourt*, 1973], on the New England shelf [*Beardsley and Butman*, 1974], off Long Island [*Scott and Csanady*, 1976], in

Paper number 2000JC000738.
0148-0227/01/2000JC000738$09.00

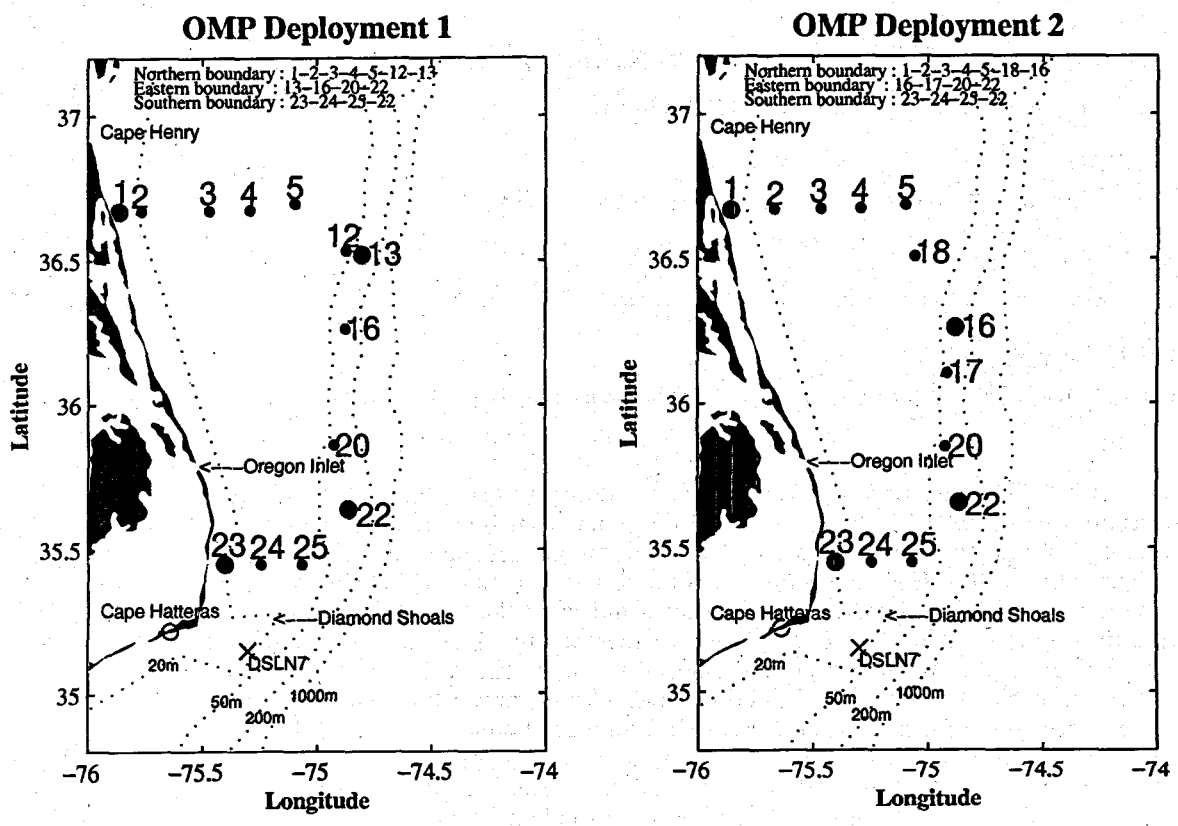

Figure 1. Locations of the Ocean Margins Program (OMP) moorings, wind (crosses), and sea level (open circles) stations and three boundaries used in this study for both deployments. The larger solid circles represent the end moorings of each boundary.

the New York Bight [*Mayer et al.*, 1979], in the MAB and on the southern flank of Georges Bank [*Noble et al.*, 1983], on the Nantucket Shoals [*Beardsley et al.*, 1985], south of Cape Cod [*Aikman et al.*, 1988], between Delaware and Chesapeake Bays [*Shaw et al.*, 1994], and north and south of Cape Hatteras [*Churchill and Berger*, 1998]. These studies indicate a mean equatorward flow on the order of 5–20 cm/s and an alongshore volume transport from the shore to the shelf edge on the MAB shelf. *Beardsley and Boicourt* [1981] and *Beardsley et al.* [1976] described the discrete data sets over a large portion of the bight. They suggested that despite the wind being stronger in winter, there was no significant seasonal variation of mean flow. The mean flow of the continental shelf in the southern MAB was to the south, approximately parallel to the local trend of isobaths. *Boicourt* [1973] and *Scott and Csanady* [1976] found a return onshore flow to compensate for the near-surface offshore flow in the middle or lower layer. *Aikman et al.* [1988] showed that the cross-shelf structure of the flow variability might be simply described as a transition from the wind-dominated outer shelf to the ocean-dominated slope region and observed that shelf water was exported to the slope in the surface and bottom boundary layers. The low-frequency motions associated with winds and movement of the shelf-slope front could affect the cross-shelf flow in the midwater column and the energy and mass exchange in the boundary layers [*Shaw et al.*, 1994]. *Beardsley and Butman* [1974] indicated that the transient alongshore flow over the shelf was generally coherent with the local alongshore wind, and the large wind-driven current and sea level fluctuations to synoptic-scale atmospheric forcing were associated with free or forced continental shelf waves [*Beardsley and Boicourt*, 1981]. *Wang* [1979] found evidence for nonlocal forcing from examination of 1 year sea level and meteorological data over the entire bight. He also investigated the relation between local wind stress and sea level in the MAB and found that the alongshore wind stress and sea level were highly coherent and that sea level lagged the local alongshore wind stress by 8–12 hours, indicating that the alongshore current and sea level fluctuations were in phase to within a few hours. *Noble and Butman* [1979] found the alongshore current consisted predominantly of wind-forced motions and freely propagating events, which together accounted for 75 ~ 90% of the alongshore current energy. *Chapman et al.* [1986] argued that the observed equatorward mean alongshelf flow in the MAB is a downstream extension of the mean alongshelf flow over the Scotian Shelf.

The shelf water moving equatorward bifurcates at the southern boundary of the OMP region, with the majority of the flow detaching from the shelf and becoming entrained in the north wall of the Gulf Stream [*Ford et al.*, 1952; *Fisher*, 1972; *Kupferman and Garfield*, 1977; *Lillibridge et al.*, 1990; *Churchill and Berger*, 1998], while a small fraction of the shelf water continues south of Cape Hatteras as the Virginia Coastal Water [*Pietrafesa et al.*, 1994]. Furthermore, the proximity of the Gulf Stream results in a complicated and potentially strong offshore forcing of the slope flow [*Bane et al.*, 1988]. Our study region was also located close to the area of nonlocal forcings (eddies and waves), which undoubtedly influence the flow over the continental slope and may affect the shelf circulation as well.

DISCLAIMER

DISCLAIMER

Portions of this document may be illegible in electronic image products. Images are produced from the best available original document.

For example, topographic Rossby waves [*Aikman et al.*, 1988] propagate away from the Gulf Stream and toward the MAB, apparently generating lower-frequency current variability over the continental shelf. Exchanges of shelf and slope water due to warm-core rings may also occur in the MAB shelf.

The continental shelf current within the study region is well known to exhibit prominent southward flow, but very little is known about the mass and salt budgets and mass and salt flux variability. The principal objectives of this study are (1) to estimate the mean volume transport and salt flux into and out of the OMP region on the basis of moored current and salinity data, (2) to examine the temporal variability of the volume transport and (turbulent) salt flux, (3) to consider the relative magnitude of the mean and turbulent salt fluxes, and (4) finally, to investigate the balance of the mean and the daily volume transports and salt fluxes.

2. Data and Methods

The data were obtained from current meters at mooring sites on the perimeter of the OMP region during two periods from middle February to early May (deployment 1) and from early July to early October (deployment 2) in 1996 (Figure 1). Moored instruments for this study were deployed over the shelf along two cross-isobath lines (the northern and the southern boundaries) and one along the 76 m along-isobath line (nominally at the shelf break) (the eastern boundary). The water depths at these moorings varied from 13 to 76 m. The northern boundary of the region extends zonally from the coast at 36°40′N, and the southern boundary extends approximately zonally from the coast at 35°27′N. The shelf moorings were outfitted with two to four of the following current meters (including temperature and conductivity sensors): SeaPac Model 2000 current meters (ACEs; Woods Hole Group, Catumet, Massachusetts), burst sampling current meters (BSCMs) [*Weatherly and Kelly*, 1982], Aanderaa recording current meters (RCMs), and S4 current meters (InterOcean System Inc., San Diego, California). Data at sites 5 and 12 of deployment 1 and at sites 5, 17, and 20 of deployment 2 were obtained by bottom-mounted acoustic Doppler current profilers (ADCPs; RDI Instrument, San Diego, California) with 1.5 ~ 2 m vertical resolution. Since currents on the shelf are highly coherent in the vertical (Figure 5; also see *Kim* [1999, Appendix A] for a quantitative description), at each ADCP, only four values at selected depths were used. The directions of current velocity data from all current meters were corrected by 11° for magnetic north variation so that 0° magnetic north corresponds to 349° true north. The data return (which was generally very good) and how data voids were filled in are discussed by *Kim* [1999]. Each moored current meter had a conductivity sensor, and adjacent to each bottom-mounted ADCP was a mooring of SeaCats conductivity-temperature recorders (Sea-Bird Electronics Inc., Bellevue, Washington). The conductivity sensor on the S4 current meter and the BSCM and ACE current meters were, respectively, those provided by the manufacturer (InterOcean System Inc., San Diego, California) and SeaBird (Sea-Bird Electronics Inc., Bellevue, Washington) SeaCat conductivity sensor.

The moored salinity data were calibrated using salinity from four conductivity-temperature-depth (CTD) surveys which were carried out during the two mooring deployments (February 4–11, 1996, and June 24–29, 1996) and the two mooring recoveries (May 8–15, 1996, and October 9–13, 1996). The CTD casts were made within 1/4 nautical mile (1 nautical mile = 1,852 km) of the moorings. From comparing the mooring salinity at each mooring site with the salinity value of the time measured from CTD casts, two CTD salinity values for the calibration of mooring salinity record were selected, and then the calibration value was decided from the average of difference between mooring and CTD salinity. In those cases where two salinity values were not available, the mooring salinity was calibrated from direct comparison of one CTD salinity value. Further details are given by *Kim* [1999].

Wind data were obtained from National Oceanic and Atmospheric Administration (NOAA) Coastal Marine Automated Network (C-MAN) station DSLN7 located in Diamond Shoals and NOAA buoy 44014 moored around Virginia Beach during the experiments. Wind stress variability of DSLN7 was similar to that of 44014 (not shown); since the distance between Virginia Beach and Diamond Shoals is small compared to the scales of the atmospheric circulation [*Shaw et al.*, 1994], the two winds should be statistically identical. Therefore only the wind data at Diamond Shoals (DSLN7) were used. The cross-shelf (τ_x) and alongshore (τ_y) wind stress were computed from

$$\tau_x = \rho_a C_d |W| U \text{ dyn/cm}^2$$

$$\tau_y = \rho_a C_d |W| V \text{ dyn/cm}^2,$$

where U and V are east (offshelf) and north (upshelf) components of wind and $|W| = (U^2 + V^2)^{1/2}$. C_d was computed according to *Wu* [1969]; that is,

$$C_d = 5 \times 10^{-5} |W|^{1/2} \qquad |W| < 1500 \text{ cm/s}$$

$$C_d = 0.0026 \qquad |W| \geq 1500 \text{ cm/s},$$

where $|W|$ is in centimeters per second and $\rho_a = 1.2 \times 10^{-3}$ g/cm^3.

The mean wind stresses for both deployments (Tables 1a and 1b) are quite representative of this region. The mean wind stress is nearly consistent with previous studies of the wind stress field in the vicinity of Chesapeake Bay of the MAB, as summarized by *Beardsley and Boicourt* [1981] and *Chuang et al.* [1979], and with the seasonal mean wind stress calculated at the northern part of MAB (~100 km west of Nantucket Shoals) by *Beardsley et al.* [1985] and *Aikman et al.* [1988].

The isobath lines of the study region are parallel to the general north-south trend of the coast, so that the current and wind stress values are presented with the x and y axes oriented toward the east (90°T) and the north (0°T), respectively. Transport values in and out of the OMP region are computed by estimating the normal flux across the straight lines connecting adjacent station pairs on the OMP perimeter rather than north-south and east-west transports across the perimeter. *Weatherly et al.* [2000] used a similar method to estimate the transport of a deep western boundary current. Sea levels from NOAA were obtained from three coastal stations at or adjacent to the study region: Chesapeake Bay, Oregon Inlet, and Cape Hatteras. The sea level data showed visual similarity among the three locations (not shown), so that sea level data at only one location, Cape Hatteras, were used in this study. The locations of the current, salinity, wind, and sea level measurements used in the analysis are shown in Figure 1.

The time series considered are the daily averaged Gaussian filtered data after smoothing by four passes with a Hanning filter (weights 1/4, 1/2, 1/4), which is equivalent to smoothing

Table 1a. Summary of Mooring Location, Water Depth, Current Meter Identification and Depth, Filtered Data Duration, Variance $\sigma^2_{v/u}$, Integral Timescale $\Im_{v/u}$ for OMP Array, and Mean Alongshore (North-South, v) and Cross-Shelf (East-West, u) Components of the Flow and the Wind Stress for Deployment 1

Time Series[a]	Position		Water Depth, m	Start–Stop (1996)[b]	Mean v/u, cm/s	$\sigma^2_{v/u}$	$\Im_{v/u}$, days
	Latitude, °N	Longitude, °W					
101A07	36°40′	−75°52′	13	02/14–05/03	−8.6/1.9	252/81	0.7/0.6
101A10	36°40′	−75°52′	13	02/14–05/03	−1.3/0.5	87/80	0.7/0.6
102A08	36°40′	−75°46′	21	02/14–05/03	−1.4/0.6	210/12	0.7/0.5
102A11	36°40′	−75°46′	21	02/14–05/03	0.7/−0.3	163/9	0.7/0.5
102A18	36°40′	−75°46′	21	02/14–05/03	1.2/−0.4	68/6	0.8/0.6
103A11	36°40′	−75°28′	28	02/14–05/03	−6.9/2.9	203/26	1.8/0.7
103A20	36°40′	−75°28′	28	02/14–05/03	−3.5/1.0	182/11	1.0/0.6
104A06	36°40′	−75°17′	23	02/14–05/03	−7.5/−1.3	237/58	0.7/0.7
104A09	36°40′	−75°17′	23	02/14–05/03	−6.9/−2.5	242/57	0.7/0.7
104A15	36°40′	−75°17′	23	02/14–05/03	−5.0/−2.0	200/17	0.7/0.7
104R20	36°40′	−75°17′	23	02/14–05/03	−2.2/−1.9	95/7	0.7/0.6
105P10	36°42′	−75°06′	29	02/14–05/03	−2.7/0.5	302/257	1.7/2.2
105P18	36°42′	−75°06′	29	02/14–05/03	−1.6/−1.3	203/84	1.6/1.6
105P24	36°42′	−75°06′	29	02/14–05/03	−1.1/−1.9	133/31	1.5/0.7
112P10	36°32′	−74°52′	40	02/14–05/03	−12.8/−3.6	197/129	1.2/1.0
112P20	36°32′	−74°52′	40	02/14–05/03	−12.0/−4.3	231/92	1.2/0.8
112P30	36°32′	−74°52′	40	02/14–05/03	−11.4/−2.7	216/57	1.2/1.1
112P35	36°32′	−74°52′	40	02/14–05/03	−9.6/−1.6	158/38	1.2/1.9
113S07	36°31′	−74°48′	76	02/14–05/03	−23.0/−0.7	546/94	2.0/1.4
113B17	36°31′	−74°48′	76	02/14–05/03	−19.6/−5.2	453/77	1.8/1.6
113B40	36°31′	−74°48′	76	02/14–05/03	−19.7/−2.0	449/38	1.8/0.8
113B71	36°31′	−74°48′	76	02/14–05/03	−12.9/−1.1	224/10	1.7/1.1
116A07	36°16′	−74°52′	76	02/22–05/03	−11.7/0.3	432/38	1.3/1.1
116B23	36°16′	−74°52′	76	02/22–05/03	−10.2/−2.2	394/40	1.3/1.2
116B37	36°16′	−74°52′	76	02/22–05/03	−10.2/−2.0	366/27	1.3/1.4
120A09	35°52′	−74°55′	76	02/22–05/03	−9.9/1.1	519/35	1.1/1.4
120P36	35°52′	−74°55′	76	02/22–05/03	−5.2/−1.2	421/13	1.5/2.0
120P56	35°52′	−74°55′	76	02/22–05/03	−5.8/0.9	377/9	1.3/0.7
120P71	35°52′	−74°55′	76	02/22–05/03	−7.2/0.7	182/23	1.2/2.2
122A09	35°38′	−74°51′	76	02/18–05/06	−5.1/9.1	392/127	1.0/1.8
122B24	35°38′	−74°51′	76	02/18–05/06	−4.4/5.1	307/77	1.1/1.6
122B38	35°38′	−74°51′	76	02/18–05/06	−5.0/4.1	274/69	1.1/1.7
122B73	35°38′	−74°51′	76	02/18–05/06	−6.3/3.5	101/75	1.1/1.1
123A07	35°27′	−75°24′	20	02/18–05/06	−6.7/−0.4	660/35	1.0/1.0
123A16	35°27′	−75°24′	20	02/18–05/06	1.0/−1.5	285/35	0.7/0.8
124A08	35°27′	−75°14′	30	02/18–05/06	−9.3/2.7	741/87	0.8/0.7
124B27	35°27′	−75°14′	30	02/18–05/06	1.1/1.1	236/25	0.8/1.2
125A07	35°27′	−75°04′	40	02/18–05/03	−3.9/12.4	756/141	1.1/0.7
125A17	35°27′	−75°04′	40	02/18–05/03	0.4/12.2	778/128	1.0/0.7
125R23	35°27′	−75°04′	40	02/18–05/03	−6.3/11.1	169/371	0.7/1.3
125S33	35°27′	−75°04′	40	02/18–05/03	3.1/6.0	284/23	1.1/1.4
Wind stress	35°09′	−75°18′	N/A	02/18–05/27	0.10/0.37 dyn/cm^2		

[a]The first numeral represents the deployment, the next two digit numeral stands for the site, the letter indicates the instrument type (P, ADCP; B, BSCM; A, ACE; R, RCM; S, S4), and the last two digit numeral indicates the depth of measurement in meters for each time series.
[b]Starting to stopping dates in 1996. Read 02/14–05/03 as February 14, 1996, to May 3, 1996.

with an 8 day low-pass filter. In the analysis, each time series was subsampled into daily data. The time series used in the analysis are labeled with the following conventions. The first numeral represents the deployment, the next two digit numeral stands for the site, the letter indicates the instrument type (P, ADCP; B, BSCM; A, ACE; R, RCM; S, S4), and the last two digit number indicates the depth of measurement in meters for each time series. Summaries of the time series of current velocity and salinity are given in Tables 1a, 1b, 2a, and 2b, where the variance σ^2 and the integral time scale $\Im$ (see section 3.1.3) were obtained from the daily averaged Gaussian-filtered data. We note that the velocity and salinity uncertainties estimated from the daily average Gaussian-filtered data are essentially the same as those estimated using the variances and the integral timescales of the 8 day low-pass data.

The discontinuities in the velocity contours and in the volume and salt flux estimates for each vertical section result from the boundaries not being straight lines and considering the normal flow component across each station pair. Vertically interpolated and extrapolated values were essentially insensitive to the particular method used; we chose linear interpolation.

3. Volume Transport and Its Balance

3.1. Mean Currents

3.1.1. Mean current vectors. The mean currents of near the surface (≈6 m from the surface), intermediate, and near the bottom (≈5 m above the bottom) of each mooring site for both deployments during the experimental periods are summarized in Figure 2 to show the vertical and horizontal flow pattern of mean currents. In the cases where four current

Table 1b. Same as Table 1a Except Deployment 2

Time Series	Position		Water Depth, m	Start–Stop (1996)	Mean v/u, cm/s	$\sigma^2_{v/u}$	$\Im_{v/u}$, days
	Latitude, °N	Longitude, °W					
201A07	36°40′	−75°51′	13	07/05–10/05	−0.8/−0.4	98/36	1.3/1.5
201A10	36°40′	−75°51′	13	07/05–10/05	0.1/−0.2	24/26	1.7/0.9
202A08	36°40′	−75°40′	18	07/05–08/26	1.6/0.8	75/19	4.3/0.7
202A15	36°40′	−75°40′	18	07/05–08/05	1.7/0.7	24/5	1.1/0.3
203A11	36°40′	−75°28′	28	07/05–10/05	−2.5/−1.0	100/33	1.9/1.3
203A20	36°40′	−75°28′	28	07/05–10/05	−1.4/1.4	76/8	1.7/0.5
204A06	36°40′	−75°17′	23	07/05–10/05	−4.3/−3.7	161/50	7.8/1.4
204A09	36°40′	−75°17′	23	07/05–10/05	−4.0/−2.9	139/37	7.2/1.5
204A15	36°40′	−75°17′	23	07/05–10/05	−5.4/−3.3	99/20	3.7/0.8
204R20	36°40′	−75°17′	23	07/05–10/05	−1.3/−1.1	16/3	1.1/0.9
205P10	36°42′	−75°06′	29	07/05–10/05	−4.2/−2.3	75/46	5.9/1.3
205P18	36°42′	−75°06′	29	07/05–10/05	−1.3/−0.4	57/23	3.9/1.3
205P24	36°42′	−75°06′	29	07/05–10/05	−1.5/0.2	40/12	2.6/1.4
216A09	36°16′	−74°53′	76	07/05–10/07	−11.1/−1.0	214/39	4.0/1.7
216B23	36°16′	−74°53′	76	07/05–10/07	−13.2/−1.1	250/18	4.1/2.5
216B37	36°16′	−74°53′	76	07/05–10/07	−12.2/−1.7	233/26	4.0/2.4
216B72	36°16′	−74°53′	76	07/05–10/07	−4.7/0.4	44/4	2.6/0.6
217A07	36°07′	−74°55′	76	07/05–10/07	−11.4/2.0	163/76	3.8/2.2
217P16	36°07′	−74°55′	76	07/05–10/07	−8.4/−2.3	186/35	3.6/1.3
217P36	36°07′	−74°55′	76	07/05–10/07	−8.3/−1.4	227/32	3.3/2.3
217P56	36°07′	−74°55′	76	07/05–10/07	−4.0/−1.2	110/27	2.6/1.6
217P69	36°07′	−74°55′	76	07/05–10/07	−3.2/−0.3	47/9	2.2/1.1
218A08	36°30′	−75°03′	38	07/05–10/05	−4.0/−2.8	63/65	3.3/2.5
218A26	36°30′	−75°03′	38	07/05–10/05	−1.6/−6.7	45/22	2.3/3.4
218R35	36°30′	−75°03′	38	07/05–10/05	0.2/−4.8	4/21	4.8/5.3
220A09	35°52′	−74°55′	76	07/05–10/07	−12.0/1.3	211/90	2.7/1.4
220P16	35°52′	−74°55′	76	07/05–10/07	−7.1/−2.1	153/31	3.0/2.8
220P36	35°52′	−74°55′	76	07/05–10/07	−6.8/−1.7	211/18	3.2/2.6
220P56	35°52′	−74°55′	76	07/05–10/07	−3.4/−0.1	151/7	2.9/1.5
220P71	35°52′	−74°55′	76	07/05–10/07	−5.9/0.4	109/7	3.2/0.8
222A09	35°39′	−74°52′	76	07/03–10/08	−3.9/4.7	186/96	1.8/1.1
222B24	35°39′	−74°52′	76	07/03–10/08	−1.0/3.6	84/55	1.1/3.0
222B73	35°39′	−74°52′	76	07/03–10/08	−4.2/2.1	38/21	0.6/2.1
223A07	35°27′	−74°24′	20	07/03–10/08	−3.7/−3.5	356/20	1.6/0.9
223A16	35°27′	−74°24′	20	07/03–10/08	0.2/0.4	156/34	1.7/1.0
224A08	35°27′	−74°14′	30	07/03–10/08	−7.2/0.5	308/68	2.3/1.7
224B27	35°27′	−74°14′	30	07/03–10/08	−1.8/0.4	47/18	1.1/0.7
225A07	35°27′	−75°04′	36	07/03–10/08	−2.6/7.3	261/216	3.3/1.5
225A17	35°27′	−75°04′	36	07/03–10/08	0.8/9.7	285/133	3.3/1.2
225R23	35°27′	−75°04′	36	07/03–09/21	−2.8/6.9	89/124	2.2/5.0
225S33	35°27′	−75°04′	36	07/03–09/12	2.3/2.7	72/28	0.9/1.3
Wind stress	35°09′	−75°18′	N/A	02/18–05/27	0.11/0.03 dyn/cm^2		

meters were on a mooring, the midlevel currents are obtained from the average of two middle-depth currents.

There are several characteristics common to both deployments. First, the mean currents are stronger near the shelf break. Second, the mean currents are generally directed alongshore toward the south except (1) in the southeast portion (moorings 22 and 25), where off-shelf, southeastward flow tends to occur, and (2) around moorings 2, 23, 24, and 5, where the flow is relatively weak and is sometimes northward. Third, there is a tendency toward stronger flows near the surface and weaker flows near the bottom with either a small onshore or offshore component generally consistent with bottom Ekman veering. The strongest mean current amplitude occurs at 7 m depth at mooring 13 and is 23.6 cm/s during the period of deployment 1 (Table 1a). Data from moorings 22 and 25 of deployment 1 and deployment 2 exhibit strong mean offshore components >9 and 5 cm/s, respectively. This offshore flow is due to transport of shelf water in a strong offshore current at the edge of the front separating MAB shelf water from the more saline shelf water of the South Atlantic Bight (SAB) as found by *Churchill and Berger* [1998]. They also suggested that export of shelf water in the southern zone of the MAB occurred over the middle and outer shelf and as indicated by 5–10 cm/s mean offshore velocities measured by current meters.

3.1.2. Vertical section of mean currents normal to the perimeter. The general flow pattern in the vertical sections for both deployments can be easily seen (Plate 1). The discontinuities appearing at certain stations in Plate 1 are due to the boundaries not being straight lines and the normal flow across the boundary being plotted. The main features in Plate 1 are a strong inflow across the northern boundary, a weak outflow at the eastern boundary, and outflow at the southern boundary that is strongest at the southeast corner between mooring 25 and 22. Southward flows are dominant at the southern boundary in the upper water column for both deployments, but near the bottom the flow is to the north at moorings 23, 24, and 25 in deployment 1 and at moorings 23 and 25 (but not 24) in deployment 2. The northward flow in the lower water column at the southern boundary may be because of the occasional appearance just above the bottom on the shelf there of an extension of the northeastward flowing Gulf Stream. The northward near-bottom flows seen at southern boundary are

Table 2a. Summary of Mooring Location, Water Depth, Instrument Identification and Depth, Filtered Data Duration for OMP Array, and Salinity Mean, Variance, Integral Timescale, and RMSU for Deployment 1[a]

Time Series	Position		Water Depth, m	Start–Stop (1996)	Mean, psu	σ^2, $(psu)^2$	$\Im$, days	RMSU, psu
	Latitude, °N	Longitude, °W						
10107	36°40′N	75°52′W	13	02/14–05/03	29.9	1.5	4	0.4
10110	36°40′N	75°52′W	13	02/14–05/03	30.6	1.1	4	0.3
10208	36°40′N	75°46′W	21	02/14–05/03	31.5	0.4	3	0.2
10211	36°40′N	75°46′W	21	02/14–05/03	33.2	0.4	4	0.3
10218	36°40′N	75°46′W	21	02/14–05/03	31.9	0.2	4	0.1
10311	36°40′N	75°28′W	28	02/14–05/03	32.8	0.2	7	0.2
10320	36°40′N	75°28′W	28	02/14–05/03	32.6	0.1	8	0.1
10406	36°40′N	75°17′W	23	02/14–05/03	33.0	0.2	6	0.2
10409	36°40′N	75°17′W	23	02/14–05/03	32.9	0.2	6	0.2
10415	36°40′N	75°17′W	23	02/14–05/03	33.1	0.1	8	0.1
10420	36°40′N	75°17′W	23	02/14–05/03	33.1	0.1	9	0.2
10510	36°42′N	75°06′W	29	02/14–05/03	33.2	0.2	8	0.2
10518	36°42′N	75°06′W	29	02/14–05/03	33.3	0.1	9	0.2
10524	36°42′N	75°06′W	29	02/14–05/03	33.3	0.1	10	0.2
11307	36°31′N	74°48′W	76	02/14–05/03	32.8	0.4	9	0.3
11317	36°31′N	74°48′W	76	02/14–04/05	33.4	0.1	6	0.2
11340	36°31′N	74°48′W	76	02/14–05/03	33.3	0.1	11	0.2
11371	36°31′N	74°48′W	76	02/14–05/03	33.6	0.2	6	0.2
11607	36°16′N	74°52′W	76	02/22–05/03	33.5	0.4	8	0.3
11623	36°16′N	74°52′W	76	02/22–03/03	33.3	0.4	1	0.3
11637	36°16′N	74°52′W	76	02/22–05/03	33.1	0.2	10	0.2
12038	35°52′N	74°55′W	76	02/22–05/03	34.3	0.7	7	0.4
12072	35°52′N	74°55′W	76	02/22–05/03	34.5	0.4	6	0.3
12224	35°38′N	74°51′W	76	02/18–05/06	33.9	0.6	5	0.3
12238	35°38′N	74°51′W	76	02/18–05/06	34.2	0.5	5	0.3
12273	35°38′N	74°51′W	76	02/18–05/06	34.0	0.3	6	0.2
12307	35°27′N	75°24′W	20	02/18–05/06	31.9	3.1	6	0.7
12316	35°27′N	75°24′W	20	02/18–05/06	32.6	2.2	5	0.5
12408	35°27′N	75°14′W	30	02/18–05/06	34.1	0.7	3	0.2
12417	35°27′N	75°14′W	30	02/18–05/06	33.6	1.6	6	0.5
12427	35°27′N	75°14′W	30	02/18–05/06	33.2	1.0	5	0.4
12507	35°27′N	75°04′W	40	02/18–05/03	34.2	1.4	5	0.4
12517	35°27′N	75°04′W	40	02/18–05/03	34.4	1.2	5	0.4
12523	35°27′N	75°04′W	40	02/18–05/03	35.1	0.4	3	0.2
12533	35°27′N	75°04′W	40	02/18–05/03	34.6	1.1	4	0.3

[a]RMSU is estimated as $(2\sigma^2\Im/T)^{1/2}$, where T is the record duration (see KWP1 for more discussion).

not found at comparable places along the northern boundary. Some northward near-bottom flow is seen at the northern boundary, but this appears only at mooring 2. As mooring 2 for deployment 2 is several kilometers farther offshore than for deployment 1 (Figure 1), the near-bottom northward flow seen in the vicinity of the 20 m isobath along the northern line appears to be a real (and puzzling) feature of the flow field rather than a localized topographic effect associated with a single mooring site. The vertical sections of mean currents for the eastern boundary indicate weak cross-shelf currents with velocity of $-5 \sim 5$ cm/s (Plate 1). Generally, the dominant flow direction is offshore (positive), so generally, the shelf water near the shelf break flows into the deeper ocean, part of which is in contact with Gulf Stream water [*Churchill and Berger*, 1998], while onshore (negative) flows are also found at the midlevel of the vertical sections between moorings 16 and 20 for deployment 1 and between moorings 17 and 20 for deployment 2 and near mooring 20.

3.1.3. Vertical section of uncertainties of mean currents normal to the perimeter. The standard error or uncertainty ε of the overall means is estimated as $\varepsilon = (2\sigma^2\Im/T)^{1/2}$, where σ^2 is the variance, T is the length of the record in days, and $\Im$ is the integral timescale in days [*Tennekes and Lumley*, 1972]. The quantity $T/(2\Im)$ is the estimate of the number of independent observations in the time series if the time series is stationary. The mean current normal to the perimeter is expected to be within the limits $\pm\varepsilon$ [*Bendat and Piersol*, 1986]. The parameter $\Im$ was estimated as the area under the autocorrelation function of the filtered current data from zero time lag to where the autocorrelation function first crosses the time lag axis (Tables 1a and 1b). On average, $\Im$ is ~1 (3) and 2 (2) days, respectively, for the alongshore and cross-shelf components of the flow for deployment 1 (2). *Aikman et al.* [1988] also obtained similar average values, 3 and 2 days, for each component of the daily current velocity data observed during >1 year in the continental shelf south of Cape Cod. Plate 2 displays the absolute value of standard error for the normal currents at each of the vertical sections for both deployments. In general, the ε values have a tendency of decreasing with depth and increasing with distance from the shore, which suggests the variances of currents decrease with increases in depth and increase with strength of currents.

3.2. Mean Volume Transport and Its Balance

3.2.1. Spatial distribution of mean volume transport. The volume transport along the northern boundary line (Figure 3) indicates, as suggested by Figure 2 and Plate 1, that much of the volume transport across this line occurs near the shelf break because that is where the alongshore currents and water depth are largest. The volume transports along the

Table 2b. Same as Table 2a Except Deployment 2

Time Series	Position		Water Depth, m	Start–Stop (1996)	Mean, psu	σ^2, $(psu)^2$	$\mathfrak{I}$, days	RMSU, psu
	Latitude, °N	Longitude, °W						
20107	36°40′N	75°51′W	13	07/05–10/05	29.8	1.7	9	0.6
20110	36°40′N	75°51′W	13	07/05–10/05	29.9	1.6	10	0.6
20208	36°40′N	75°40′W	18	07/05–08/26	31.5	0.4	6	0.3
20215	36°40′N	75°40′W	18	07/05–08/05	32.0	0.1	4	0.2
20311	36°40′N	75°28′W	28	07/05–10/05	31.0	0.3	12	0.3
20320	36°40′N	75°28′W	28	07/05–10/05	31.6	0.3	11	0.3
20406	36°40′N	75°17′W	23	07/05–10/05	30.6	0.1	4	0.1
20409	36°40′N	75°17′W	23	07/05–10/05	31.1	0.2	8	0.2
20415	36°40′N	75°17′W	23	07/05–10/05	31.9	0.3	12	0.3
20420	36°40′N	75°17′W	23	07/05–10/05	31.3	1.3	6	0.4
21609	36°16′N	74°53′W	76	07/05–09/01	31.7	0.8	6	0.2
21623	36°16′N	74°53′W	76	07/05–10/07	33.0	0.3	7	0.2
21672	36°16′N	74°53′W	76	07/05–10/07	32.9	0.5	9	0.3
21707	36°07′N	74°55′W	76	07/05–10/07	32.1	1.2	7	0.2
21722	36°07′N	74°55′W	76	07/05–10/07	32.5	0.8	8	0.4
21737	36°07′N	74°55′W	76	07/05–10/07	32.6	0.5	9	0.3
21772	36°07′N	74°55′W	76	07/05–10/07	33.0	0.8	10	0.4
21808	36°30′N	75°03′W	38	07/05–10/05	32.2	0.6	7	0.3
21826	36°30′N	75°03′W	38	07/05–10/05	32.2	0.3	8	0.2
21835	36°30′N	75°03′W	38	07/05–10/05	32.3	0.2	10	0.2
22209	35°39′N	74°52′W	76	07/03–10/08	33.2	2.9	7	0.6
22239	35°39′N	74°52′W	76	07/03–10/08	33.6	1.7	6	0.5
22273	35°39′N	74°52′W	76	07/03–10/08	33.7	0.7	8	0.3
22307	35°27′N	74°24′W	20	07/03–08/17	32.7	2.6	5	0.6
22316	35°27′N	74°24′W	20	07/03–10/08	30.6	3.9	7	0.6
22408	35°27′N	74°14′W	30	07/03–10/08	32.2	3.1	10	0.8
22427	35°27′N	74°14′W	30	07/03–10/08	33.8	2.4	5	0.5
22507	35°27′N	75°04′W	36	07/03–10/08	33.2	3.4	11	0.9
22517	35°27′N	75°04′W	36	07/03–10/08	34.4	2.9	9	0.7
22523	35°27′N	75°04′W	36	07/03–09/21	34.1	1.8	8	0.6
22533	35°27′N	75°04′W	36	07/03–09/12	34.8	2.8	6	0.7

northern boundary line are essentially directed southward (negative) for both deployments because of the southward currents at moorings 5, 12, and 13 (for deployment 1) and at moorings 5, 18, and 16 (for deployment 2). The volume transport along the southern boundary (Figure 3) indicates, as implied in Figure 2 and Plate 1, that much of the volume transport across this line occurs near the eastern portion and is directed toward the southeast. The volume transport at the eastern boundary indicates net offshore transport (positive values) for both deployments, which is smaller in magnitude than the transports across the other boundaries. Comparing the volume transport across each section for deployment 1 with that for deployment 2 (Figure 3) indicates that they were larger in magnitude for deployment 1.

3.2.2. Mass balance with uncertainty. The cumulative volume transports (hereafter CVTs) (Figure 4) are calculated from the area integrals of the average current velocities normal to the vertical sections of each boundary for both deployments (Plate 1). The irregular shapes of the boundaries are due to some mooring sites not having sufficient data necessary for the volume transport calculation. The CVT uncertainty across each boundary line is estimated as the area integral of the uncertainty in the mean velocities (Plate 2). Comparing deployment 2 with deployment 1 (Figure 4), the uncertainties of deployment 2 show a relatively larger fraction of uncertainty because of a smaller CVT at each boundary (Figure 4).

The CVTs in Figure 4 are all equatorward at the northern and southern boundaries and vary from 0.13 ± 0.07 (for deployment 2) to 0.17 ± 0.07 Sv (for deployment 1) at the northern boundary and from 0.09 ± 0.05 (for deployment 2) to 0.14 ± 0.05 Sv (for deployment 1) at the southern boundary. The CVTs at the eastern boundary are to the offshore and vary from 0.05 ± 0.06 Sv (for deployment 2) to 0.08 ± 0.07 Sv (for deployment 1). The greater mean CVTs for deployment 1 may be real and due to seasonal variation in the mean wind stress. Note that the mean wind stress for deployment 1, which includes the winter and spring seasons, is ~3 times that for deployment 2, which includes the summer and fall seasons (Tables 1a and 1b).

Our alongshelf volume transports across the northern and southern boundary lines (Figure 4) compare favorably with those of *Churchill and Berger* [1998] (0.17 Sv out to 100 m isobath), *Biscaye et al.* [1994] (0.19 Sv out to 130 m isobath), and *Beardsley et al.* [1976] (0.26 Sv out to 100 m isobath), and the cross-shelf volume transport at the eastern boundary line of the shelf break (Figure 4) compares favorably with the instantaneous value found by *Kupferman and Garfield* [1977]. The southern boundary was divided into two parts, a western part (moorings 23, 24, and 25) and an eastern part (moorings 25 and 22) to allow us to determine the percentage of CVT flowing out of the southeast corner region. At the southeast corner the flow directions veer offshore (Figure 2), and a relatively large amount of water flows out of this region (Figure 4). The CVT for the southeast corner region accounts for 74% (0.11 Sv) and 67% (0.06 Sv) of the flow out of the southern boundary in deployments 1 and 2, respectively, which suggests that the southeast corner has a significant role in the mass budget. At the western part of the southern boundary, there is a relatively small amount of southward flow, which may extend into Raleigh Bay and, occasionally, Onslow Bay as noted by

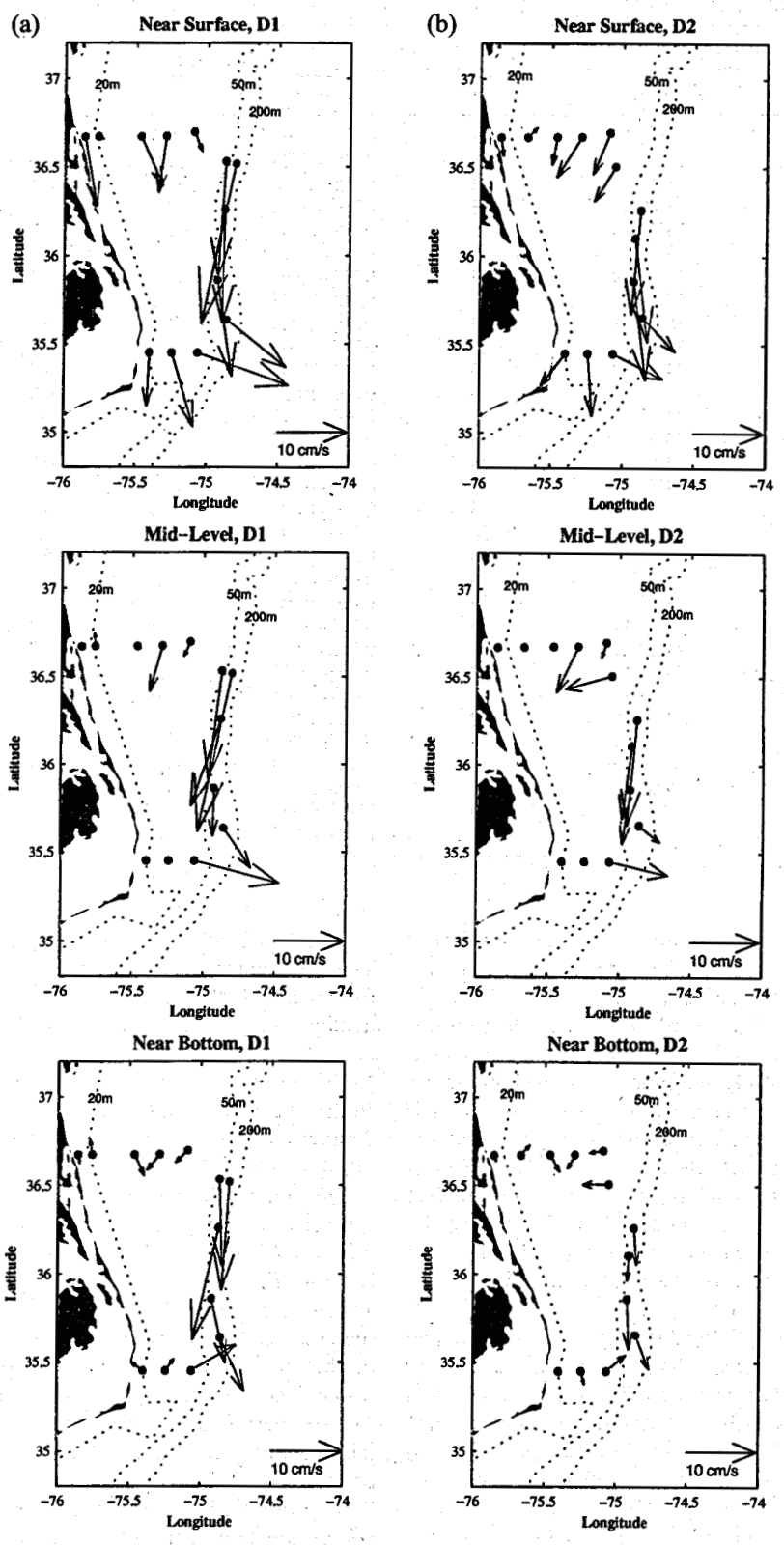

Figure 2. Record mean currents at near-surface, midlevel and near-bottom layers for (a) deployment 1 (D1) and (b) deployment 2 (D2).

Pietrafesa et al. [1994]. They indicated that the minimum net CVT of MAB water around Cape Hatteras into the SAB is 0.025 Sv, which favorably agrees with our estimates (0.037 Sv for deployment 1 and 0.028 Sv for deployment 2).

The general impression from the CVTs in Figure 4 is that most of what comes in the northern boundary goes out the southern boundary with the remainder going out the eastern boundary. Further, most of what leaves across the southern

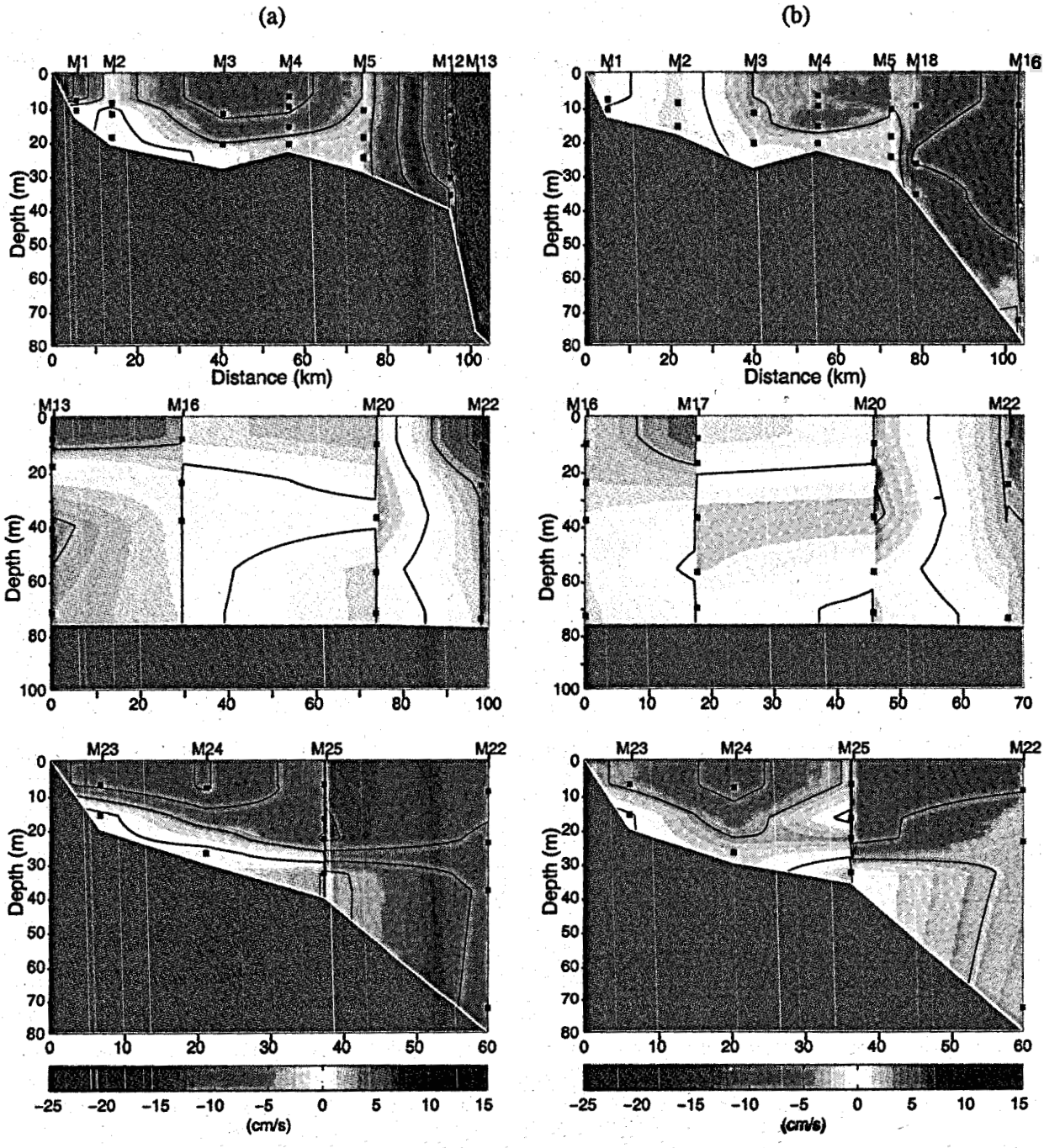

Plate 1. Contours of record mean currents normal to the vertical section for (a) deployment 1 and (b) deployment 2. Locations of instruments are indicated by solid squares, and mooring numbers are shown at the top. Distance is measured from the shore at the northern and southern boundaries and from northern mooring at the eastern boundary. Contour interval is 3 cm/s. (top) northern section, (middle) eastern section, and (bottom) southern section.

boundary does so in the eastern corner, and this outflow has a pronounced offshore component. The above impression is reinforced when the uncertainties are included except for the eastern boundary during deployment 2. As a result, mass balances in the closed volume of both deployments are satisfied within the range of uncertainty.

3.3. Variability of Volume Transport

3.3.1. Currents. During the periods of both deployments the velocity fields in the study region were dominated by events of strong currents lasting from 7 to 31 days (Figure 5). There were several events of southward currents. Most events could be identified at all sites. There were also periods of northward currents in the study region. Some current variations agreed with the variations in wind stress; however, this was not always the case. A weak southward wind stress corresponded to a strong southward flow, while a strong northward wind stress produced a weak northward flow. The flow was sometimes southward when the wind stress was northward. Therefore, in

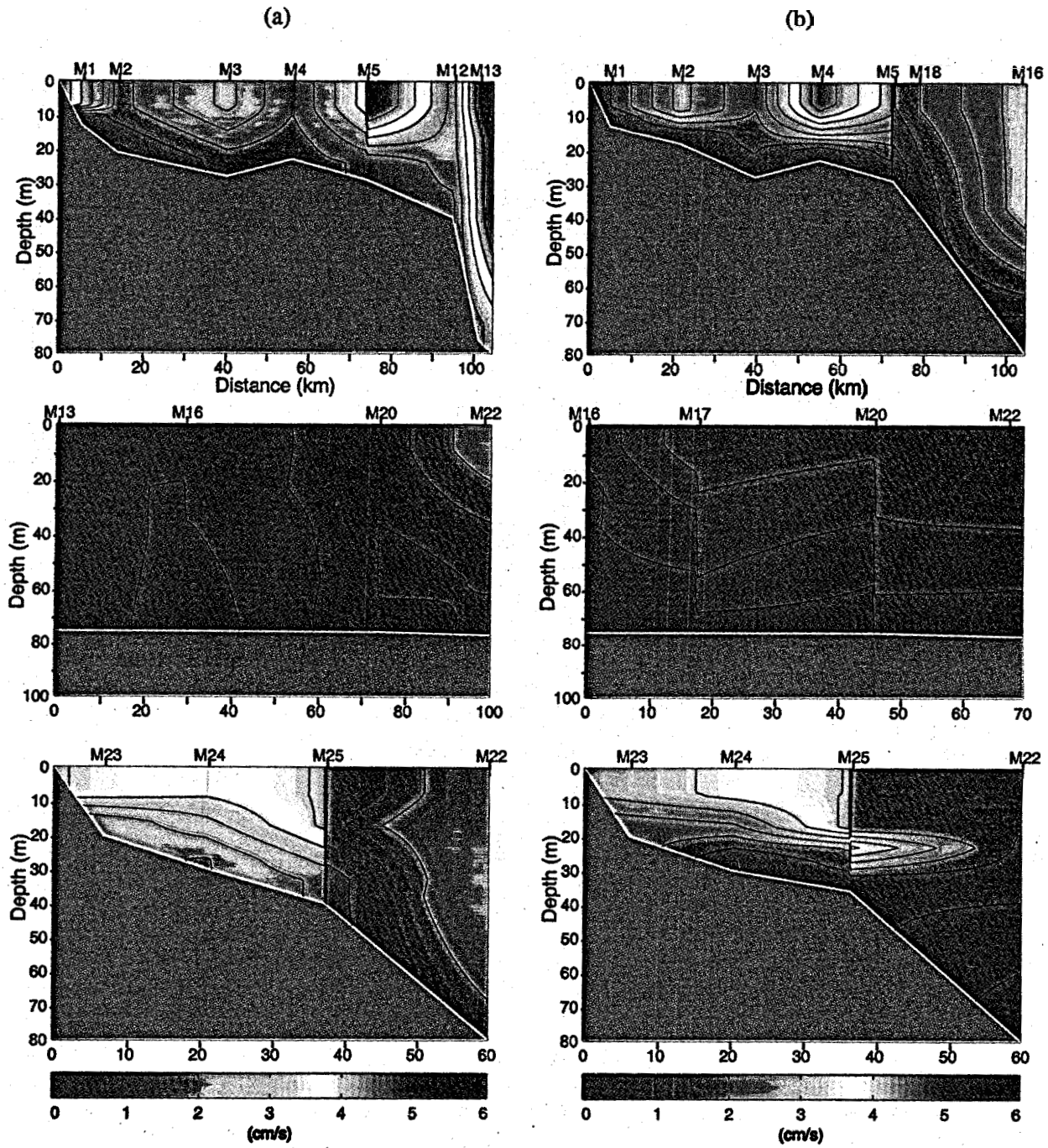

Plate 2. Contours of positive RMSE values to calculate uncertainties of the cumulative volume transports for (a) deployment 1 and (b) deployment 2. Contour interval is 0.5 cm/s.

agreement with results presented in section 3.2, the wind-induced fluctuations appear to be superimposed upon a mean southward flow.

Currents associated with wind-driven events showed some depth variations. Sometimes the near-bottom current vectors were less than and oriented counterclockwise to the middle-depth (when available) and the surface current vectors, which indicates that the near-bottom currents were influenced by bottom friction. On the contrary, such behavior is not as evident during deployment 1 at moorings 12, 13, and 16, where the fluctuations are more uniform with depth. In general, more vertical variation with depth is evident in deployment 2. The vertical variations at the southeast corner, moorings 22 and 25 and, sometimes, in the eastern side at moorings 18 (deployment 2) and 20 show a more complicated structure that is related to their proximity to the Gulf Stream.

Currents associated with wind events, which are oriented approximately alongshore, appear to vary nearly barotropically at each mooring and more so for deployment 1 than deployment 2 (Figure 5). EOF analysis (not shown here, but shown by *Kim* [1999]) confirms that the current fluctuations across the northern and southern boundaries were indeed very (80–90%) barotropic. This analysis also indicates that normal flow across the eastern boundary was less (40% or more) barotropic.

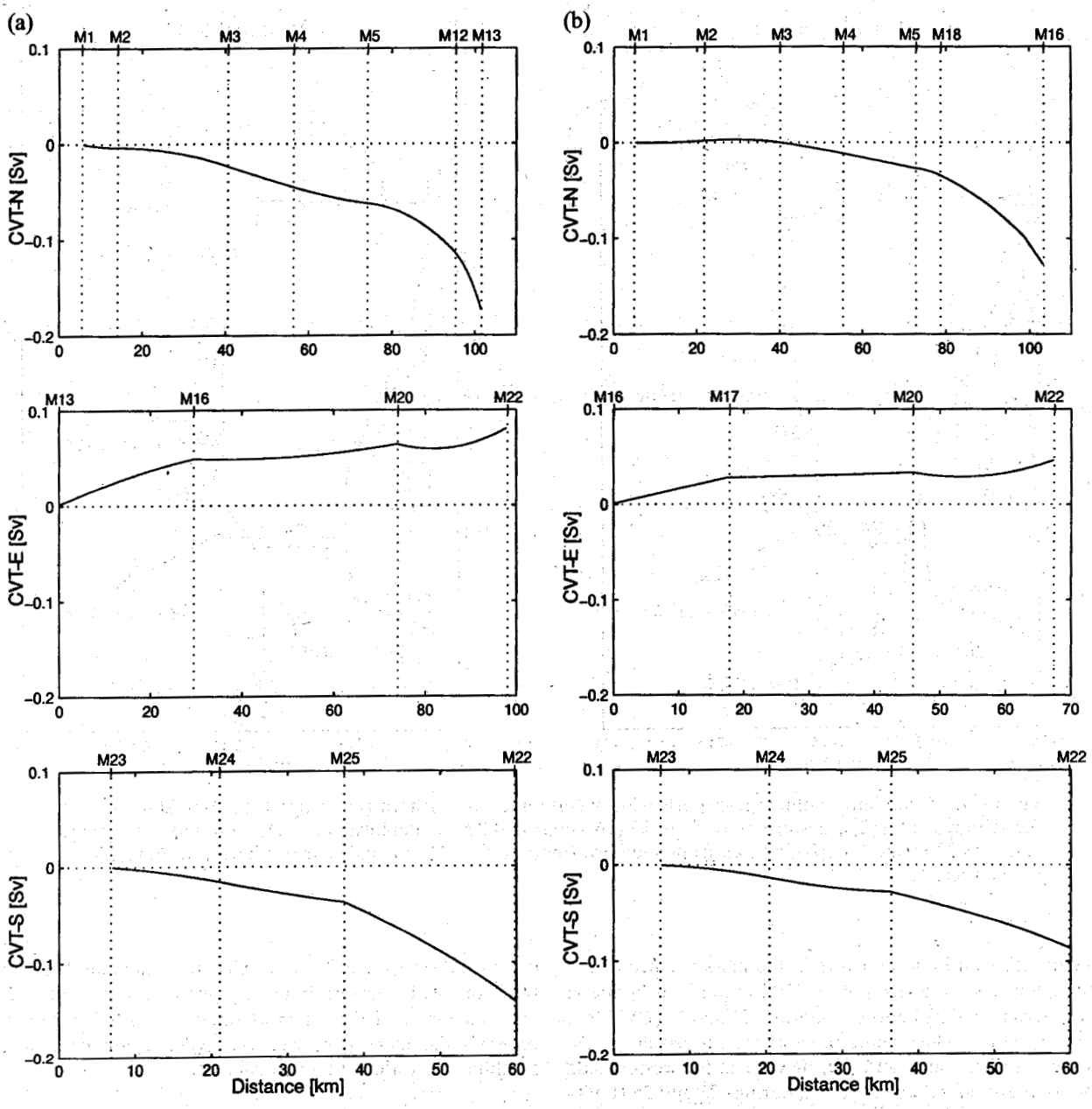

Figure 3. Mean cumulative volume transports with distance for (a) deployment 1 and (b) deployment 2.

3.3.2. Cumulative volume transport time series. The daily time series of CVTs (CVT-N, the CVT at the northern boundary, CVT-E, the CVT at the eastern boundary, and CVT-S, the CVT at the southern boundary) for both deployments were obtained from the integral of the filtered daily currents normal to the vertical section described in Section 3.1.1 (Figure 6). The alongshore CVTs (CVT-N and CVT-S) for both deployments are visually highly correlated and in phase with each other. They appeared to be 180° out of phase with sea level fluctuations. In other words, sea level increase is associated with a southward volume transport, which suggests a geostrophic balance between the cross-shelf pressure gradient and alongshore current. The fluctuations of CVT-E are generally 180° out of phase with those of alongshore CVTs (especially for deployment 1), implying that a southward (northward) alongshore flow at the northern and southern boundaries creates an eastward (westward) flow at the eastern boundary. This flow pattern is weaker during the period of deployment 2, which includes the summer season, because of stronger westward reversing flow at the middle and lower layers. The time series of the CVT-N shows that the transport varies by ~1.0 Sv (from ~0.4 to ~−0.6 Sv); thus the amplitude of the variable transport is more than twice the magnitude of the mean (southward) transport (~0.2 Sv). Similarly, the transport extends northward as well as southward at the southern boundary, where the southward and northward flows can be partly explained by variable wind forcing [*Kim*, 1999] and the movement of the Hatteras front [*Churchill and Berger*, 1998], which separates the MAB and SAB shelf water masses and cuts across the middle shelf in the Diamond Shoals region. While a relatively small amount of shelf water flows in or out across the eastern boundary with time, we will see later that the eastern

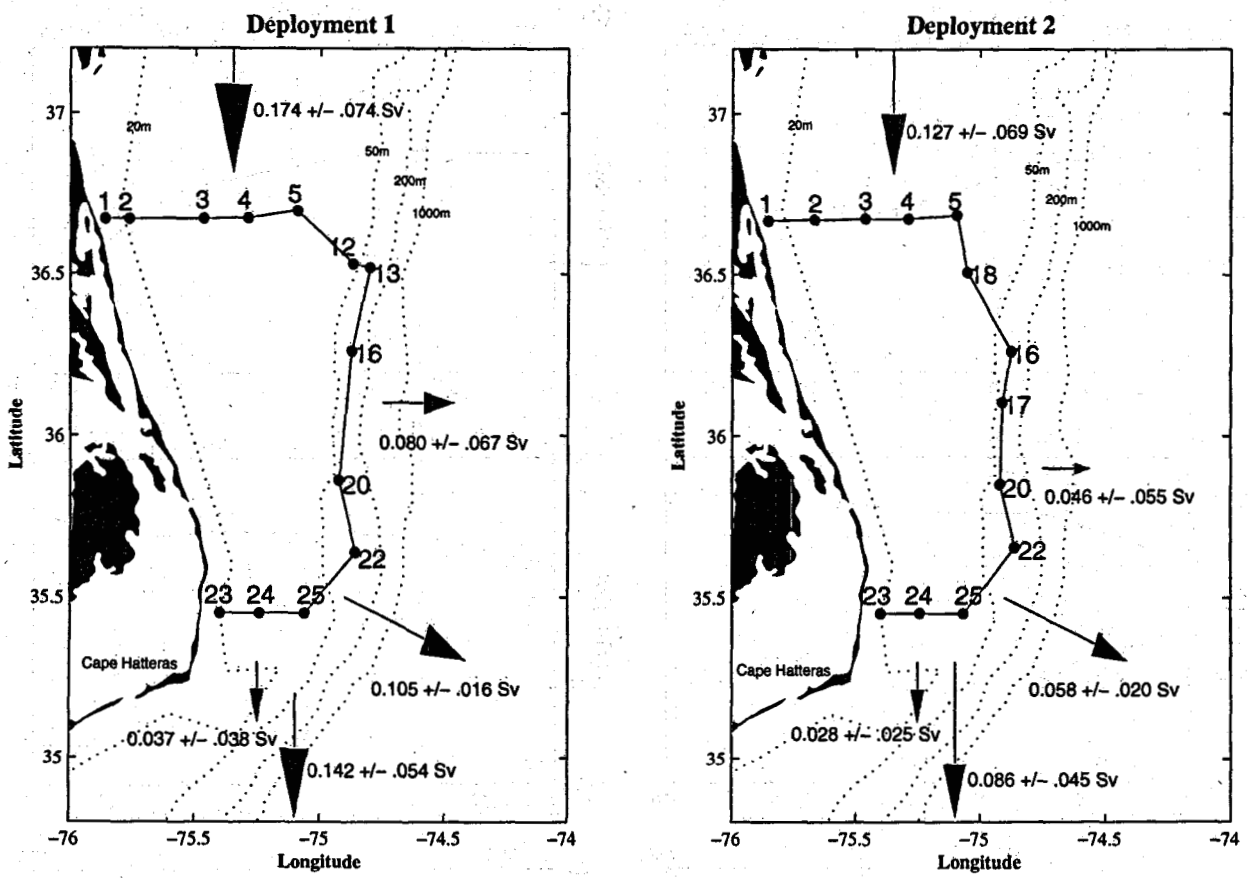

Figure 4. Cumulative volume transports with uncertainties at northern (moorings 1-2-3-4-5-12(18)-13(16) for deployment 1(2)), eastern (moorings 13-(16)-16(17)-20-22 for deployment 1(2)), southern (moorings 23-24-25-22 for both deployments), front southern (moorings 23-24-25), and rear southern (mooring 25-22) boundaries.

boundary plays an important role in the mass balance of the OMP region. The time series of the CVT at the eastern side of the southern boundary between moorings 25 and 22 (CVT-RS) indicate negative values and strong southeastward flows. On the other hand, the time series of the CVT at the western side of the southern boundary between moorings 23 and 25 (CVT-FS) show more frequent oscillations toward both the north and the south, implying that there is water exchange between the MAB and SAB. *Pietrafesa et al.* [1994] found, from 7 years of data collected at Diamond Shoals, that for >50% of the year, there could be significant leakage of MAB water into the SAB around Cape Hatteras when the wind is blowing from the north.

3.4. Mass Balance

In order to show the role of mass balance the difference between alongshore CVTs (CVT-N minus CVT-S) with time was compared with time series of CVT-E (east) (Figure 7). Figure 7 shows that when the values of CVT-N − CVT-S are positive (negative), those of CVT-E tend to be negative (positive), and when southward CVT across the northern (southern) boundary is bigger than that across the southern (northern) boundary, CVT-N − CVT-S < 0 (CVT-N − CVT-S > 0) eastward (westward) CVT-E occurs across the eastern boundary. In other words, when southward CVT-N is greater than southward CVT-S, shelf water export at the eastern boundary occurs and vices versa. Therefore it can be said that the volume transport at the eastern boundary plays an important role in mass balance and that at most times during the OMP field program the moored current observations are of sufficient resolution to estimate a mass balance.

4. Salt Flux and Its Balance

As background, the mean salinity for each section is shown in Plate 3 (the salinity time series used to form Plate 3 are shown by *Kim* [1999]). Plate 3 shows that (1) low-salinity Chesapeake and Delaware Bay waters are found in the near-shore region on the northern and southern sections and this is more pronounced for deployment 2, which includes the summer season when the river runoff is larger; (2) high-salinity water is found in the southeast part of the study region because of the proximity of the Gulf Stream; (3) the mean salinity for both deployments increases going offshore and southward in the OMP region; and (4) there is stronger vertical stratification in deployment 2, especially in the eastern portion of the southern boundary of the study region. Associated with points 1 and 4, results presented by *Kim*'s [1999] Figure 28 indicate a two-layer structure in the cross-shelf velocity for deployment 2 in the southeast corner of the study region.

At any moment, the cumulative salt flux (CSF) across a section is

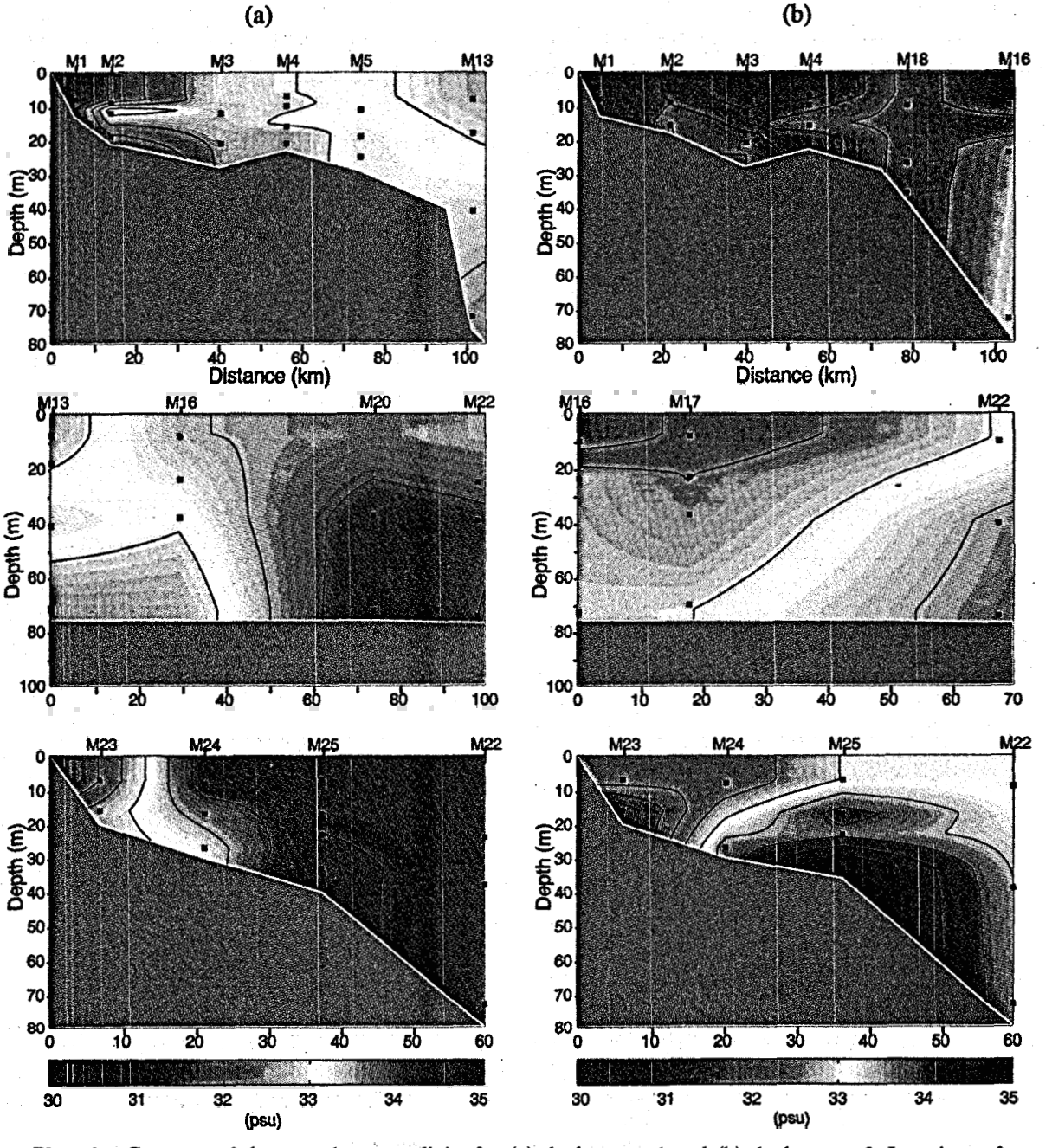

Plate 3. Contours of the record mean salinity for (a) deployment 1 and (b) deployment 2. Locations of instruments are indicated by solid squares, and mooring numbers are shown at the top. Distance is measured from the shore at the northern and southern boundaries and from northern mooring at the eastern boundary. Contour interval is 0.5 psu. (top) northern section, (middle) eastern section, and (bottom) southern section.

$$\mathrm{CSF}(t) = \int_0^w \int_{-h}^0 v_n(x, z, t) S(x, z, t)\, dz\, dx, \qquad (1)$$

where $v_n(x, z, t)$ is the velocity normal to the vertical section, $S(x, z, t)$ is the salinity, h is the water depth, w is the section width; x is the horizontal coordinate, z is the vertical coordinate, and t is time. The CSF(t) for each section are shown in Figure 8. It is apparent comparing Figure 8 to the respective CVT(t) in Figure 6 that the CSF(t) are very similar in appearance to the CVT(t), suggesting that the salt flux is primarily determined by the velocity field.

Decomposing according to $v_n(x, z, t) = \overline{v_n}(x, z) + v_n'(x, z, t)$ and $S(x, z, t) = \bar{S}(x, z) + S'(x, z, t)$, where the overbar denotes a time average and the prime denotes a deviation from the time average, and time averaging (1) yields the average cumulative salt flux

$$\overline{\mathrm{CSF}} = \int_0^w \int_{-h}^0 (\overline{v_n}\bar{S} + \overline{v_n'S'})\, dz\, dx. \qquad (2)$$

Both terms on the right-hand side of (2) are shown for each section for each deployment in Figure 9. It is apparent that

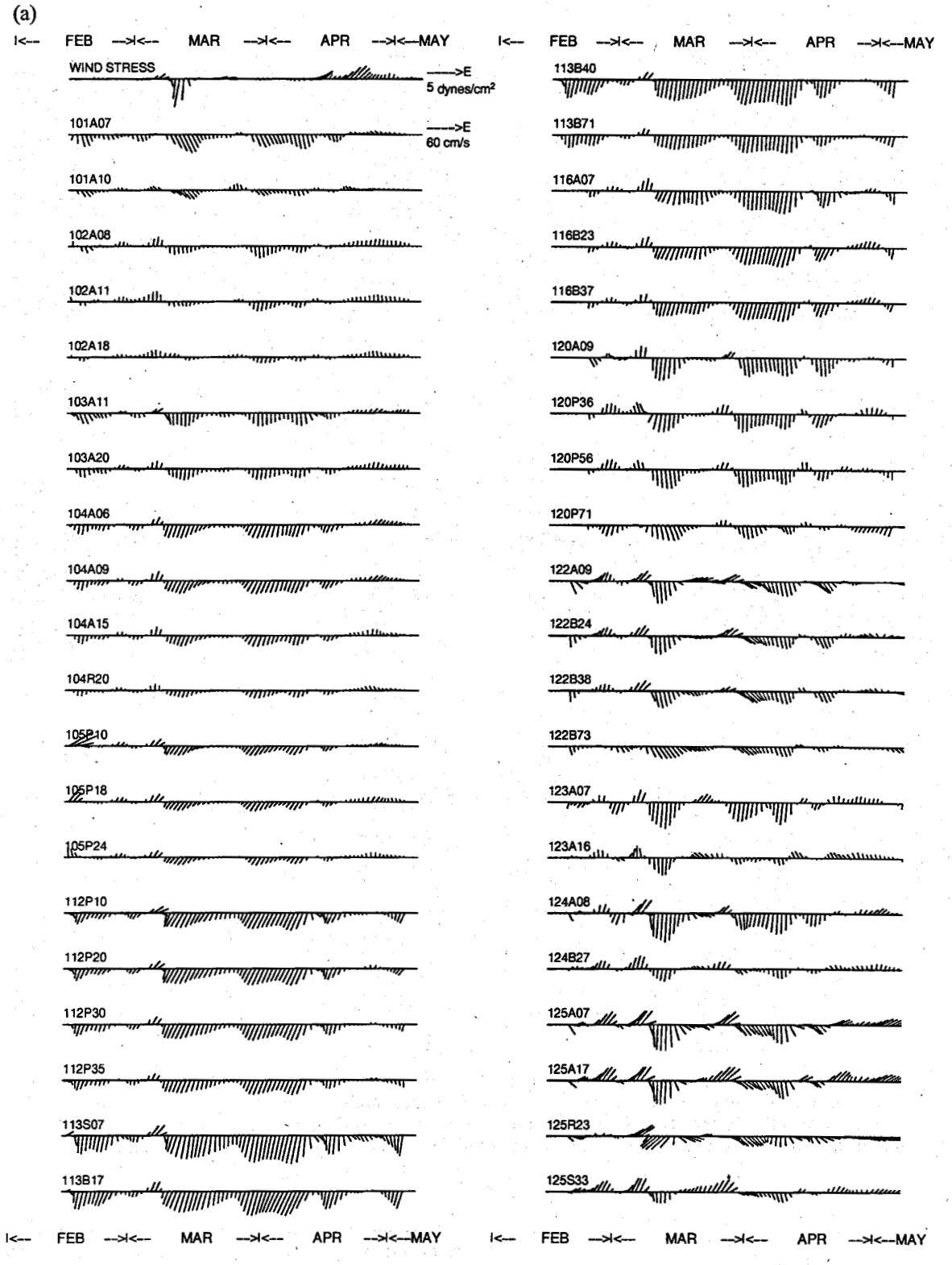

Figure 5. (a) Composite stick plots of the current meter records from mooring locations of Table 1a. Values are daily average ones after subsequent four passes with a Hanning filter (weight 1/4, 1/2, 1/4), equivalent to smoothing with an 8 day low-pass filter. (b) Composite stick plots of the current meter records from mooring locations of Table 1b. Values are daily average ones after subsequent four passes with a Hanning filter (weight 1/4, 1/2, 1/4), equivalent to smoothing with an 8 day low-pass filter.

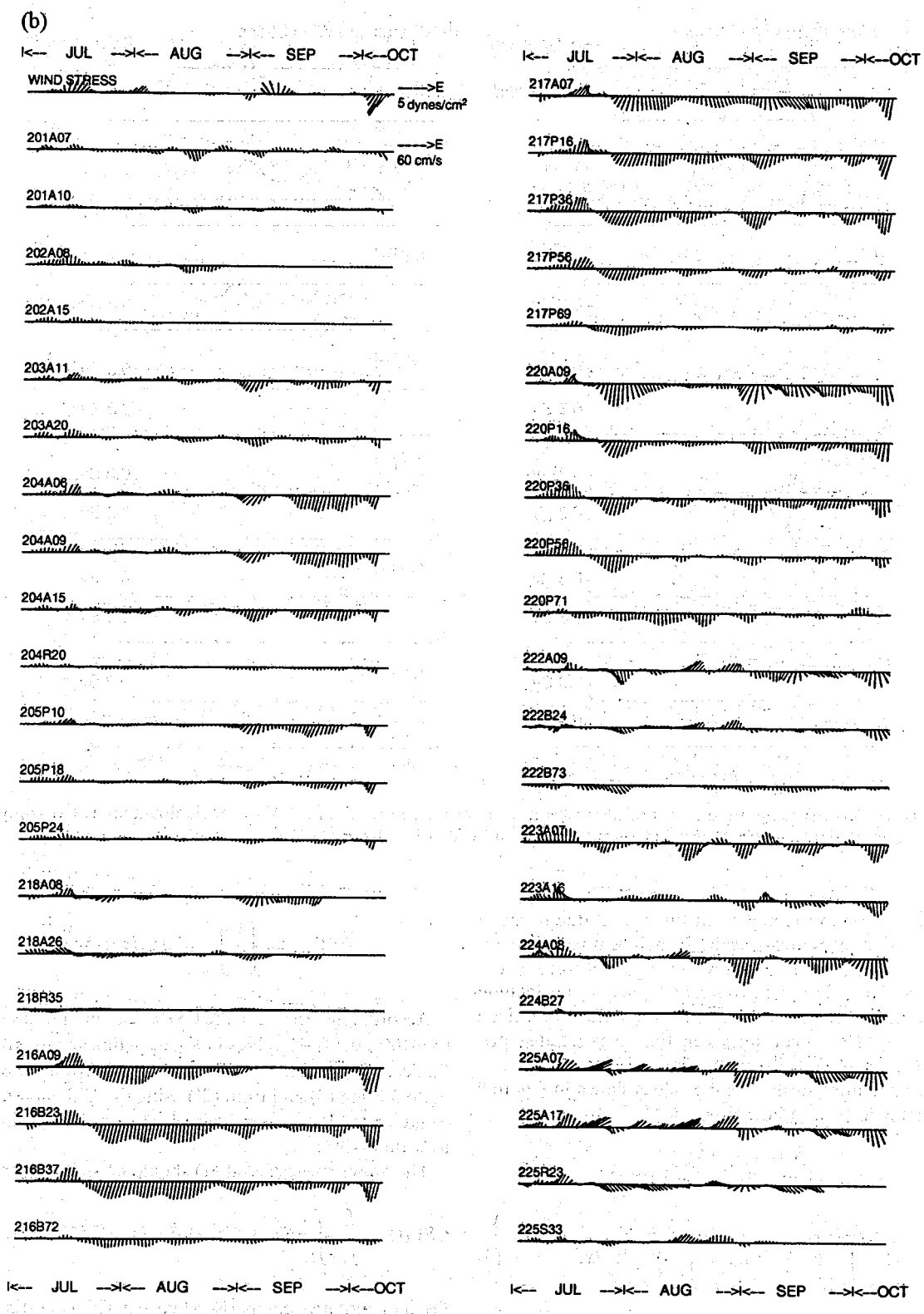

Figure 5. (continued)

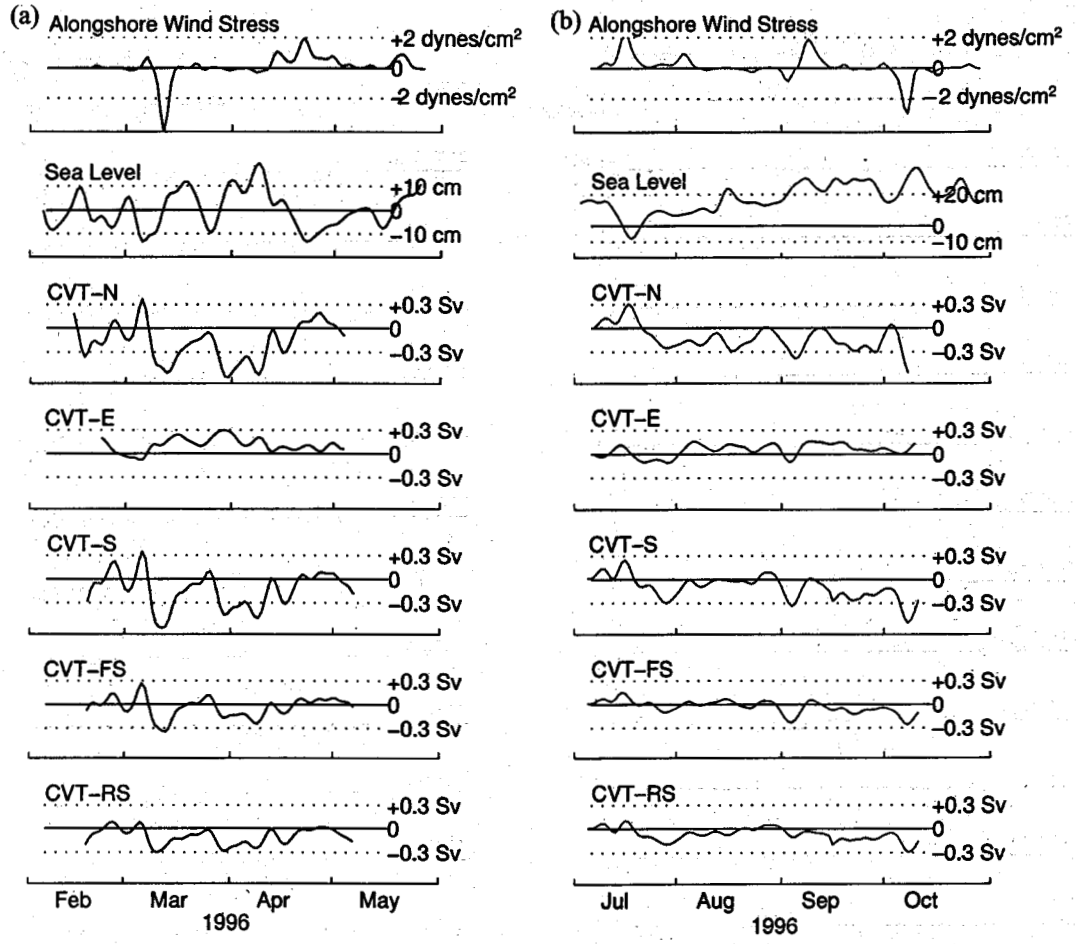

Figure 6. (a) Daily time series of alongshore wind stress, sea level, and CVTs for deployment 1. (b) Daily time series of alongshore wind stress, sea level, and CVTs for deployment 2.

the dominant term in the mean salt flux is that due to mean velocity and salt fields and that the turbulent fluxes contribute <1%. The uncertainties shown in Figure 9 were calculated in a manner similar to those in Figure 4 and include the uncertainty in the mean salinities; the details are given by *Kim* [1999]. The uncertainties in Figure 9 are due primarily to the mean velocity uncertainties [*Kim*, 1999].

Before commenting further on the values shown in Figure 9 we note that $\bar{S}$ in (2) can be expressed

$$\bar{S} = \overline{S_o} + \delta\overline{S_o},$$

where

$$\overline{S_o} \equiv \int_0^w \int_{-h}^0 \bar{S}\, dz\, dx \Big/ \int_0^w \int_{-h}^0 dz\, dx, \qquad (3)$$

where $\overline{S_o}$ is the section average salinity and where $\delta\overline{S_o}$ is the deviation of $\overline{S}$ from $\overline{S_o}$.Neglecting the turbulent salt flux in (2) and using (3) yields

$$\overline{\mathrm{CSF}} \approx \overline{S_o} \int_0^w \int_{-h}^0 \overline{v_n} \left(1 + \frac{\delta\overline{S_o}(x, z)}{\overline{S_o}}\right) dz\, dx. \qquad (2')$$

From Plate 3, $|\delta\overline{S_o}|/\overline{S_o} \lesssim 0.1$. Thus to within ~10% (2′) can be approximated by

$$\overline{\mathrm{CSF}} \approx \overline{S_o} \int_0^w \int_{-h}^0 \overline{v_n}\, dz\, dx = \overline{S_o}\ \overline{\mathrm{CVT}}. \qquad (2'')$$

Accordingly, from (2″), the $\overline{\mathrm{CSF}}$ values in Figure 9 should be, to ≤10%, the $\overline{\mathrm{CVT}}$ values in Figure 4 times the corresponding $\overline{S_o}$. As a test of this, we have estimated $\overline{S_o}$ from the $\bar{S}$ shown in Plate 3 using (3) and from (2′) using the $\overline{\mathrm{CSF}}$ shown in Figure 9 and the $\overline{\mathrm{CVT}}$ shown in Figure 4. These values (Table 3) agree to within ≈3%.

The above suggests that (1) should be well approximated by

$$\mathrm{CSF}(t) \approx \int_0^w \int_{-h}^0 \overline{S_o} v_n(x, z, t)\, dz\, dx \equiv \overline{S_o}\ \mathrm{CVT}(t). \qquad (1')$$

For a quantitative comparison between CSF(t) estimated from (1) and from (1′) we used the index of agreement parameter I_a of *Willmott et al.* [1985] and *Suh et al.* [1994]. I_a is given by

$$I_a = 1 - \frac{\sum_{j=1}^{N} |P_j - Q_j|}{\sum_{j=1}^{N} (|P_j - \bar{Q}| + |Q_j - \bar{Q}|)}, \qquad (4)$$

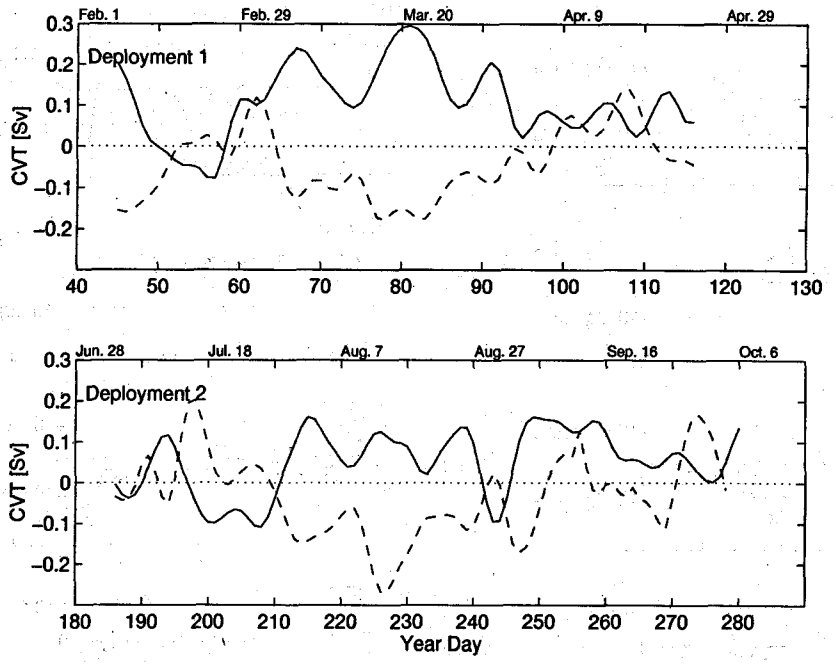

Figure 7. Relationship between CVT-N − CVT-S (dashed line) and CVT-E (solid line) for both deployments.

where P_j are CSF_j estimated from (1'), Q_j are the CSF_j estimated from (1), and $\bar{Q} = \overline{CSF}$ estimated from (1). Note that $0 \le I_a \le 1$ and that zero represents poor agreement and 1 represents perfect agreement. The I_a values we estimated were all ≥0.98, implying that (1') is a very good approximation to (1).

We do not show contours of $\overline{v_n S} + \overline{v_n' S'} \approx \overline{v_n S}$ for each section (they are shown by *Kim* [1999]) because they are virtually identical in appearance to the contours of $\overline{v_n}$ plots Plate 1. Similarly, we do not show time series plots of CSF(t) for the north section minus the CSF(t) for the south section superposed over the CSF(t) plot for the eastern section for both deployments (they are given by *Kim* [1999]) as they are, again, virtually identical in appearance to the CVT-N − CVT-S and CVT-E plots shown in Figure 7.

5. Discussion and Summary

The mean currents for both deployments are generally to the south, alongshore, and stronger near the shelf break. There are exceptions: (1) at the inner region of shelf (moorings 2, 5, 23, and 24), where weak and sometimes northward flow occurs, and (2) the southeast corner region (moorings 22 and 25), which has (strong) off-shelf, southeast flow. From this mean flow structure, the mean volume transports were estimated. The mean volume transports indicates southward, alongshore transports at the northern and southern boundaries with large offshore transport at the southeast corner region, and weak offshore transport at the eastern boundary.

Figures 3 and 4 summarized the mean mass budget inferred from moored current meter records. About 0.15 (±0.07) Sv, the average of both deployments, enters the OMP continental shelf region from the north, with most of this (≈65%) occurring near the shelf break where the currents are stronger and the water is deeper. About 45% of the water leaving the OMP region exits at the southeast corner region as a rather strong seaward flow. About 35% leaves on the eastern edge as a broad, diffuse eastward flow, and the remaining (≈20%) leaves along the southwest corner as a weak equatorward coastal current. We note that for both deployments, within the uncertainties of the volume transport estimates, all the water entering the OMP region from the northern boundary can be accounted for by the seaward flow in the southeast corner region between moorings 22 and 25.

A mean mass balance in the OMP region for both deployments is obtained within the uncertainties of the CVT estimates (Figure 4). The uncertainties for CVTs have similar values for both deployments, unlike the mean CVT values that are larger for deployment 1. Considering the uncertainties, there is clearly inflow for both deployments across the northern boundary and outflow for both deployments across the southeast corner and outflow across the eastern boundary for deployment 1. While essentially zero transport is possible across the western part of the southern boundary for both deployments and for the eastern boundary for deployment 2, if there is mean flow across these boundaries, an outflow seems more likely.

The mean wind stress during the period of deployment 1, which includes the winter season, is ~3 times stronger than that during the period of deployment 2. The mean alongshore CVTs (CVT-N and CVT-S) for deployment 1 are not as large, 50–100%, compared to those for deployment 2. However, the difference in the mean alongshore CVTs between deployments 1 and 2 is not significant when the uncertainties are considered (Figure 4). This is consistent with the suggestion that seasonal variation in the alongshore transport is small [*Beardsley et al.*, 1976]. The mean CVT-E of deployment 1 is ~2 times larger than that of deployment 2. The length of the eastern side for deployment 1 (98 km) is only ~46% longer than it is in deployment 2 (67 km), so the difference cannot be attributed to geometrical effects. The difference in the mean CVT-Es across

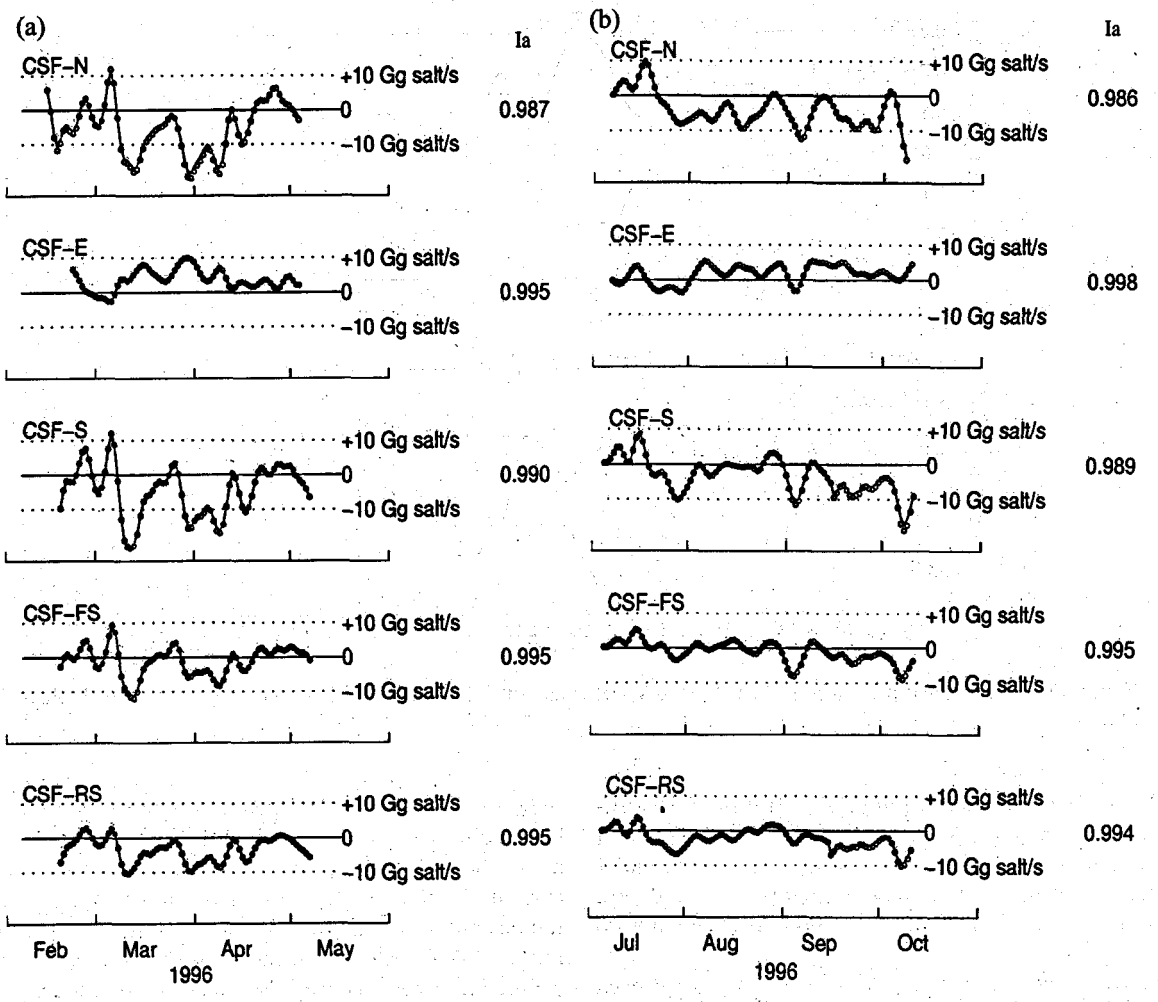

Figure 8. (a) Daily time series of CSFs (solid line) and the product of daily time series of CVT times section averaged salinity (open circles) for deployment 1. Ia is Index of agreement. Gg is 10^9 grams. (b) Daily time series of CSFs (solid line) and the product of daily time series of CVT times section averaged salinity (open circles) for deployment 2. Ia is Index of agreement. Gg is 10^9 grams.

the eastern boundary line, if real, is probably due to the weaker mean wind forcing during deployment 2. However, when the uncertainties are considered, the difference in the CVT-Es between the two deployments is not significant.

The CVT-N and CVT-S time series are visually very similar to each other (Figure 6). (Cross spectra (not shown here, but shown by *Kim* [1999]) confirm this similarity.) Also CVT-N and CVT-S time variations appear to be out of phase with coastal sea level fluctuations (Figure 6) consistent with a geostrophic balance. This inverse variability of the alongshore CVTs with sea level is also confirmed by cross spectra (not shown here, but shown by *Kim* [1999]). That the time series of the CVT-N and CVT-S are related to the wind stress variability is not as clearly apparent in Figure 6; the wind stresses are visually dominated in Figure 6 by storm events. However, cross spectra of CVT-N and CVT-S with the wind stress (not shown here, but shown by *Kim* [1999]) indicate the alongshore transports are, as expected, highly coherent with the alongshore wind stress and lag it by a few hours.

The across-slope volume transport variations at the eastern boundary CVT-E are less visually related to CVT-N and to CVT-S than CVT-N and CVT-S are related to each other (Figure 6). That CVT-E is related to the alongshore transports is more evident in Figure 7. Figure 7 shows that when there is net inflow or outflow into the region in the alongshore direction (CVT-N − CVT-S > 0 or < 0), there is generally a net outflow or inflow across the eastern boundary (CVT-E > 0 or < 0). This pattern is upheld (1) in a mean sense in Figure 7, which indicates that not all the influx through the northern boundary goes out through the southern boundary and that the remainder goes out through the eastern boundary, and (2) in a statistical sense in cross spectra of CVT-E with CVT-N (CVT-S) [*Kim*, 1999]. Thus CVT-E can be regarded as a tuning factor for the mass balance.

On the average, the net outflow exceeds the inflow by 0.066 and 0.023 Sv for deployments 1 and 2, respectively. We think this excess inflow over outflow is not significant within the uncertainties. The freshwater input from Oregon Inlet (Figure 1) is negligibly small (of the order of 10^{-4} Sv) [*Jarrett*, 1976], and the OMP region is one where there is a net small loss from evaporation and precipitation [*Schmitt*, 1994]. The excess inflow is probably due to CVT-E being overestimated. We think the transport across the eastern boundary is the least well determined because unlike the northern and southern bound-

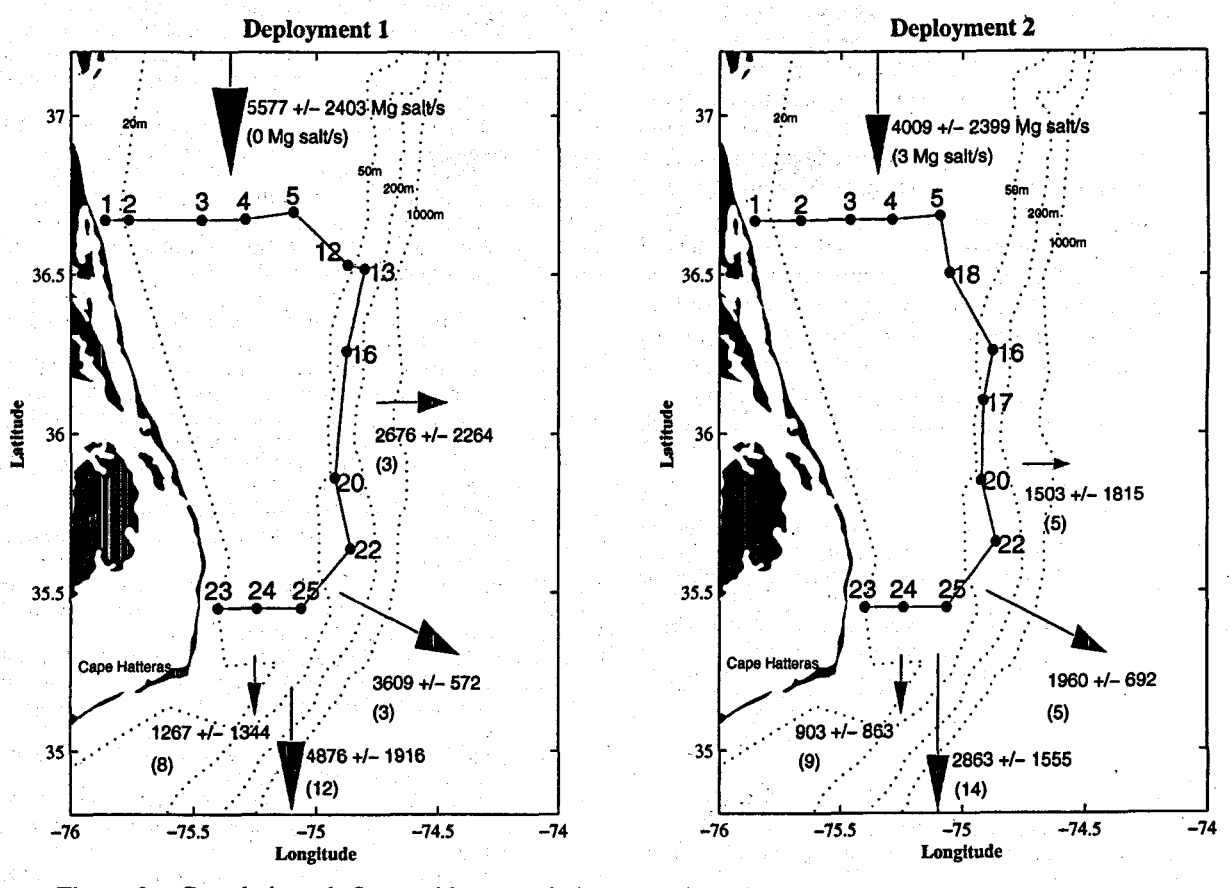

Figure 9. Cumulative salt fluxes with uncertainties at northern (moorings 1-2-3-4-5-12(18)-13(16) for deployment 1(2)), eastern (moorings 13-(16)-16(17)-20-22 for deployment 1(2)), southern (moorings 23-24-25-22 for both deployments), front southern (moorings 23-24-25), and rear southern (mooring 25-22) boundaries. The values in the parenthesis represent mean cumulative turbulent salt fluxes. Mg is 10^6 grams.

aries, the mean currents there are nearly parallel rather than normal to the line. The CVT there is relatively sensitive on how the side is chosen.

The turbulent salt fluxes across each boundary were found to play a minor role (Figure 9) in the salt fluxes. This is expected as the magnitude of the turbulent salinity fluctuations ($\lesssim$1 psu) were much less than the representative salinities ($\approx$32 psu), even though the turbulent velocity fluctuations were comparable to the mean velocities. The time series of the salt fluxes across each boundary (CSF(t)) were very similar in appearance to the time series of the volume fluxes (CVT(t)) which indicates that the salt flux is determined by the velocity field. It was found that CSF(t) and $\overline{\text{CSF}}$ across each boundary were well approximated by CVT(t)$\overline{S_o}$ and $\overline{\text{CVT}}\,\overline{S_o}$, respectively, where $\overline{S_o}$ is the deployment average salinity across the boundary.

The OMP moored current and salinity observations appear sufficient to make estimates of the mean and time-dependent mass and salt balances. These observations indicate that on average, about two thirds of the mass and salt fluxes entering the OMP shelf region across its northern boundary exits across its southern boundary with the remaining one third exiting to the open ocean as a broad, diffusive flow across the eastern, seaward boundary.

The mean velocity vectors together with the main volume transports and salt fluxes suggest that ~70% of the export across the southern boundary goes to the open ocean because

Table 3. Section Average Salinity $\overline{S_o}$ for Deployments 1 and 2[a]

	$\overline{S_o}$ for Deployment 1, psu		$\overline{S_o}$ for Deployment 2, psu	
	Estimated From (2′)	Estimated From (3)	Estimated From (2′)	Estimated From (3)
Northern boundary	32.0	32.0	31.6	31.1 (1.6%)
Southern boundary	34.3	34.3	32.5	33.3 (2.5%)
Eastern boundary	33.5	33.5	32.7	32.7

[a]Values in parentheses are percent differences when the two estimates differ.

of a strong, southward flow in the southeast corner of the OMP region. If correct, this implies that ~80% of the shelf water entering the OMP region from the north is exported to the open sea. We believe there is, indeed, a net seaward transport of shelf water at the southeast corner but that it is not as large as the 80% estimate above suggests. Estimation of the current meter time series from the southeast corner region (Figure 5, moorings 22 and 25) indicates that a mean southeastward flow results for some current meters due to an actual southeastward flow (e.g., record 225R23 in Figure 5), while for others it is due to a southward flow averaged with an occasional northeast flow due to a Gulf Stream excursion (e.g., record 222A09 in Figure 5). Further study is required to better quantify the export of shelf waters in the southeast corner of our study region to see which fraction continues southward along the shelf and which fraction is exported to the open ocean.

Acknowledgments. We wish to extend our thanks to the Current Meter Facilities at the Florida State University and at the North Carolina State University for their excellent efforts in obtaining the data and to the captain and crew of the R/V *Oceanus* for their excellent assistance in the mooring cruises. We thank R. Harkema and J. Epps for their assistance in the data processing. This investigation was supported by the Department of Energy (grants DE-FG05-92ER61416 (G.L.W.) and DE-FG09-85ER60376 (L.J.P.)) and the National Science Foundation (grant OCE-9730120).

References

Aikman, F., H. W. Ou, and R. W. Houghton, Current variability across the New England continental shelf-break and slope, *Cont. Shelf Res.*, *8*, 625–651, 1988.

Bane, J. M., Jr., O. B. Brown, R. H. Evans, and P. Hamilton, Gulf Stream remote forcing of shelfbreak currents in the Mid-Atlantic Bight, *Geophys. Res. Lett.*, *15*, 405–407, 1988.

Beardsley, R. C., and W. C. Boicourt, On estuarine and continental shelf circulation in the Middle Atlantic Bight, in *Evolution of Physical Oceanography*, edited by B. A. Warren and C. Wunsch, pp. 198–234, MIT Press, Cambridge, Mass., 1981.

Beardsley, R. C., and B. Butman, Circulation on the New England continental shelf: Response to strong winter storms, *Geophys. Res. Lett.*, *1*, 181–184, 1974.

Beardsley, R. C., W. C. Boicourt, and D. V. Hansen, Physical oceanography of the Middle Atlantic Bight, special symposia, *Am. Soc. Limnol. Oceanogr.*, *2*, 20–34, 1976.

Beardsley, R. C., D. C. Chapman, and K. H. Brink, The Nantucket Shoals Flux Experiment (NSFE79), part 1, A basic description of the current and temperature variability, *J. Phys. Oceanogr.*, *15*, 713–748, 1985.

Bendat, J. S., and A. G. Piersol, *Random Data: Analysis and Measurement Procedures*, 566 pp., Wiley-Interscience, New York, 1986.

Biscaye, P. E., C. N. Flagg, and P. G. Falkowski, The Shelf Edge Exchange Processes on the Southern Middle Atlantic Bight: SEEP-II, *Deep Sea Res., Part II*, *41*, 231–252, 1994.

Boicourt, W. C., The circulation of water on the continental shelf from Chesapeake Bay to Cape Hatteras, Ph.D. thesis, 183 pp., Johns Hopkins University, Baltimore, Md., 1973.

Chapman, D. C., J. A. Barth, R. C. Beardsley, and R. G. Fairbanks, On the continuity of mean flow between the Scotian Shelf and the Middle Atlantic Bight, *J. Phys. Oceanogr.*, *16*, 758–772, 1986.

Chuang, W.-S., D.-P. Wang, and W. C. Boicourt, Low-frequency current variability on the southern Mid-Atlantic Bight, *J. Phys. Oceanogr.*, *9*, 1144–1154, 1979.

Churchill, J. H., and T. J. Berger, Transport of Middle Atlantic Bight shelf water to the Gulf Stream near Cape Hatteras, *J. Geophys. Res.*, *103*, 30,605–30,621, 1998.

Fisher, A., Jr., Entrainment of shelf water by the Gulf Stream northeast of Cape Hatteras, *J. Geophys. Res.*, *77*, 3248–3255, 1972.

Ford, W. L., J. R. Longard, and R. E. Banks, On the nature, occurrence and origin of cold low salinity water along the edge of the Gulf Stream, *J. Mar. Res.*, *11*, 281–293, 1952.

Jarrett, J. T., Tidal prism-inlet area relationships, *GITI Rep. No. 3*, U.S. Army Coastal Eng. Res. Cent., Fort Belvoir, Va., 1976.

Kim, Y. Y., Mass and salt budgets and saline water intrusions for a region of the continental shelf in the southern Mid-Atlantic Bight, Ph.D. thesis, 116 pp., Fla. State University, Tallahassee, 1999.

Kupferman, S. L., and N. Garfield, Transport of low-salinity water at the slope water-Gulf Stream boundary, *J. Geophys. Res.*, *82*, 3481–3486, 1977.

Lee, T. N., and E. Williams, Wind-forced transport fluctuations of Florida Current, *J. Phys. Oceanogr.*, *18*, 937–946, 1988.

Lillibridge, J. L., III, G. Hitchcock, T. Rossby, E. Lessard, M. Mork, and L. Golmen, Entrainment and mixing of shelf/slope waters in the near-surface Gulf Stream, *J. Geophys. Res.*, *95*, 13,065–13,087, 1990.

Mayer, D. A., D. V. Hansen, and D. Ortman, Long-term current and temperature observations on the Middle Atlantic Shelf, *J. Geophys. Res.*, *84*, 1776–1792, 1979.

Noble, M., and B. Butman, Low-frequency wind-induced sea level oscillations along the east coast of North America, *J. Geophys. Res.*, *84*, 3227–3236, 1979.

Noble, M., B. Butman, and E. Williams, On the alongshelf structure of subtidal currents on the eastern United States Continental Shelf, *J. Phys. Oceanogr.*, *13*, 2125–2147, 1983.

Pietrafesa, L. J., J. M. Morrison, M. P. McCann, J. H. Churchill, E. Bohm, and R. W. Houghton, Water mass linkages between the Middle and South Atlantic Bights, *Deep Sea Res., Part II*, *41*, 365–389, 1994.

Scott, J. T., and G. T. Csanady, Nearshore current off Long Island, *J. Geophys. Res.*, *81*, 5401–5409, 1976.

Schmitt, R. W., The ocean freshwater cycle, *Rep. 4*, 32 pp., Ocean Observing System Development Panel Background, Texas A&M Univ., College Station, 1994.

Shaw, P.-T., L. J. Pietrafesa, C. N. Flagg, R. W. Houghton, and K.-H. Su, Low-frequency oscillations on the outer shelf in the southern Mid-Atlantic Bight, *Deep Sea Res., Part II*, *41*, 253–271, 1994.

Suh, K. D., Y. Y. Kim, and D. Y. Lee, Equilibrium-range spectrum of waves propagating on currents, *J. Waterw. Port Coastal Ocean Eng.*, *120*, 434–450, 1994.

Tennekes, H., and J. L. Lumley, *A First Course in Turbulence*, 300 pp., MIT Press, Cambridge, Mass., 1972.

Wang, D.-P., Low frequency sea level variability on the Middle Atlantic Bight, *J. Mar. Res.*, *37*, 683–697, 1979.

Weatherly, G. L., and E. A. Kelley, Too cold bottom layers at the base of the Scotian Rise, *J. Mar. Res.*, *40*, 985–1012, 1982.

Weatherly, G. L., Y. Y. Kim, and E. A. Kontar, Eulerian measurements of the North Atlantic Deep Water Deep Western Boundary Current at 18°S, *J. Phys. Oceanogr.*, *30*, 971–986, 2000.

Willmott, C. J., S. G. Ackleson, R. E. Davis, J. J. Feddema, K. M. Klink, D. R. Legates, J. O'Donnel, and C. M. Rowe, Statistics for the evaluation and comparison of models, *J. Geophys. Res.*, *90*, 8995–9005, 1985.

Wright, W. R., and C. E. Parker, A volumetric temperature/salinity census for the Middle Atlantic Bight, *Limnol. Oceanogr.*, *21*, 563–571, 1976.

Wu, J., Windstress and surface roughness at the air-sea interface, *J. Geophys. Res.*, *74*, 444–445, 1969.

Y. Y. Kim, Department of Meteorology, Florida State University, Tallahassee, FL 32306, USA.

L. J. Pietrafesa, Department of Marine, Earth and Atmospheric Sciences, North Carolina State University, Raleigh, NC 27695, USA.

G. L. Weatherly, Department of Oceanography, Florida State University, Tallahassee, FL 32306, USA. (weatherly@ocean.fsu.edu)

(Received November 27, 2000; revised April 23, 2001; accepted June 19, 2001.)